large variation (Figure 4). In the relationship between CBF and $CMRO_2$, all ROIs in the right hemisphere showed severely decreased $CMRO_2$ (Figure 5). These results indicated that the compensatory mechanism at 1 h after MCAO onset had collapsed at 24 h and the progression of ischemic injury was severer than at 1 h.

In Figure 6 and Table 2, quantitative values and standard deviations of CBF, OEF and $CMRO_2$ are summarized. In the right hemisphere, CBF decreased slightly at 1 h and severely at 24 h. Both values were significantly low compared with the opposite sides ($P<0.05$) at both time points and the difference between the 24 h was also significant ($P<0.05$). In the left hemisphere, CBF showed a little decrease but was not significant during 24 h ($P=0.0865$). Since $CMRO_2$ expressed exactly the same values at both time points, the decrease in CBF might not mean a metabolic dysfunction but a vascular disturbance at 24 h. Although blood vessels in the left hemisphere should not be affected directly in our MCAO operation, the progression of the ischemic damage in the right hemisphere included both the spreading of the ischemic core and the disturbance of surrounding blood vessels so that it is considered that the decrease in CBF on the opposite side could have occurred. Furthermore, $CMRO_2$ in the left hemisphere was close to the value obtained previously in normal rats using ^{133}Xe as a CBF tracer and a surgical method for determining OEF (6.3 ± 0.3 mL/min/100 g) (Kozniewska and Szczepanska-Sadowska, 1990). It underlined the preceding discussion that the brain tissue in the left hemisphere was not damaged at all during 24 h and the reason for the little decrease in CBF was vascular disturbance.

In the right hemisphere, $CMRO_2$ decreased severely during 24 h in the same manner as CBF (Figure 6, Table 2). Since these values did not represent $CMRO_2$ in the ischemic core but just values in the entire right hemisphere because of the large size of ROIs, it is difficult to discuss the progression of impairment. However, taken together with the decreases in CBF in both hemispheres during 24 h, the decrease in $CMRO_2$ might not mean an ischemic core-specific progression of tissue disturbance but a spreading of the ischemic damage throughout the hemisphere. In fact, TTC staining revealed no sign of disturbance at 1 h but severe disruption at 24 h in the right hemisphere.

Meanwhile, an obvious change of OEF was also evident during 24 h (Figure 6, Table 2). The increase in OEF in the right hemisphere compared with the left side at 1 h after the onset of MCAO ($P<0.05$) showed that the metabolic compensatory mechanism was working well. However, at 24 h, the OEF was the same in both hemispheres ($P=0.7532$), which indicates that the compensatory mechanism did not function at 24 h after the onset. Therefore, considering that the condition in the left hemisphere at 1 h was actually normal or stage I in the course of the ischemic disorder (Nemoto *et al*, 2004; Powers, 1991), the right hemisphere at 1 h might include partly stage II and stage III (Figures 2 and 3; CBF was normal or decreased, OEF increased and $CMRO_2$ was normal or slightly decreased), the left hemisphere at 24 h might be expressed at stage II (Figures 4 and 5; CBF decreased, OEF increased, $CMRO_2$ was normal) and the right hemisphere at 24 h might include early and severe phases of stage III (Figures 4 and 5; CBF decreased, OEF increased or decreased and $CMRO_2$ strikingly decreased).

Conclusion

In this paper, we estimated the changes in CBF, OEF and $CMRO_2$ after the onset of MCA occlusion in rats by PET using injectable ^{15}O-O_2. In the early phase after occlusion, a decrease in CBF and compensatory increase in OEF were shown, and in contrast, CBF and $CMRO_2$ were severely decreased in the late phase. This is the first report to indicate reliable oxygen metabolism in a MCAO rat model using PET.

References

Baron JC (2001) Perfusion thresholds in human cerebral ischemia: historical perspective and therapeutic implications. *Cerebrovasc Dis* 11(Suppl 1):2–8

Belayev L, Zhao W, Busto R, Ginsberg MD (1997) Transient middle cerebral artery occlusion by intraluminal suture: I. Three-dimensional autoradiographic image-analysis of local cerebral glucose metabolism–blood flow interrelationships during ischemia and early recirculation. *J Cereb Blood Flow Metab* 17:1266–80

Derejko M, Slawek J, Lass P, Nyka WM (2001) Cerebral blood flow changes in Parkinson's disease associated with dementia. *Nucl Med Rev Cent East Eur* 4:123–7

Ginsberg MD (2003) Adventures in the pathophysiology of brain ischemia: penumbra, gene expression, neuroprotection: the 2002 Thomas Willis Lecture. *Stroke* 34:214–23

Heiss WD, Graf R, Lottgen J, Ohta K, Fujita T, Wagner R *et al* (1997) Repeat positron emission tomographic studies in transient middle cerebral artery occlusion in cats: residual perfusion and efficacy of postischemic reperfusion. *J Cereb Blood Flow Metab* 17:388–400

Heiss WD, Graf R, Wienhard K, Lottgen J, Saito R, Fujita T *et al* (1994) Dynamic penumbra demonstrated by sequential multitracer PET after middle cerebral artery occlusion in cats. *J Cereb Blood Flow Metab* 14:892–902

Heiss WD, Kracht LW, Thiel A, Grond M, Pawlik G (2001) Penumbral probability thresholds of cortical flumazenil binding and blood flow predicting tissue outcome in patients with cerebral ischaemia. *Brain* 124:20–9

Kozniewska E, Szczepanska-Sadowska E (1990) V2-like receptors mediate cerebral blood flow increase following vasopressin administration in rats. *J Cardiovasc Pharmacol* 15:579–85

Kuge Y, Minematsu K, Yamaguchi T, Miyake Y (1995) Nylon monofilament for intraluminal middle cerebral artery occlusion in rats. *Stroke* 26:1655–8

Longa EZ, Weinstein PR, Carlson S, Cummins R (1989) Reversible middle cerebral artery occlusion without craniectomy in rats. *Stroke* 20:84–91

Magata Y, Temma T, Iida H, Ogawa M, Mukai T, Iida Y *et al* (2003) Development of injectable O-15 oxygen and estimation of rat OEF. *J Cereb Blood Flow Metab* 23: 671–6

Minematsu K, Li L, Fisher M, Sotak CH, Davis MA, Fiandaca MS (1992) Diffusion-weighted magnetic resonance imaging: rapid and quantitative detection of focal brain ischemia. *Neurology* 42:235–40

Mintun MA, Raichle ME, Martin WR, Herscovitch P (1984) Brain oxygen utilization measured with O-15 radiotracers and positron emission tomography. *J Nucl Med* 25:177–87

Mori S (2002) Responses to donepezil in Alzheimer's disease and Parkinson's disease. *Ann NY Acad Sci* 977: 493–500

Nemoto EM, Yonas H, Kuwabara H, Pindzola RR, Sashin D, Meltzer CC *et al* (2004) Identification of hemodynamic compromise by cerebrovascular reserve and oxygen extraction fraction in occlusive vascular disease. *J Cereb Blood Flow Metab* 24:1081–9

Pappata S, Fiorelli M, Rommel T, Hartmann A, Dettmers C, Yamaguchi T *et al* (1993) PET study of changes in local brain hemodynamics and oxygen metabolism after unilateral middle cerebral artery occlusion in baboons. *J Cereb Blood Flow Metab* 13: 416–24

Powers WJ (1991) Cerebral hemodynamics in ischemic cerebrovascular disease. *Ann Neurol* 29:231–40

Shidahara M, Watabe H, Kim KM, Oka H, Sago M, Hayashi T *et al* (2002) Evaluation of a commercial PET tomograph-based system for the quantitative assessment of rCBF, rOEF and $rCMRO_2$ by using sequential administration of ^{15}O-labeled compounds. *Ann Nucl Med* 16:317–27

Takamatsu H, Tsukada H, Kakiuchi T, Nishiyama S, Noda A, Umemura K (2000) Detection of reperfusion injury using PET in a monkey model of cerebral ischemia. *J Nucl Med* 41:1409–16

Temma T, Magata Y, Mukai T, Kitano H, Konishi J, Saji H (2004) Availability of *N*-isopropyl-p-[(125)I]iodoamphetamine (IMP) as a practical cerebral blood flow (CBF) indicator in rats. *Nucl Med Biol* 31:811–4

Tenjin H, Ueda S, Mizukawa N, Imahori Y, Hino A, Ohmori Y *et al* (1992) Positron emission tomographic measurement of acute hemodynamic changes in primate middle cerebral artery occlusion. *Neurol Med Chir (Tokyo)* 32:805–10

Walovitch RC, Cheesman EH, Maheu LJ, Hall KM (1994) Studies of the retention mechanism of the brain perfusion imaging agent 99mTc-bicisate (99mTc-ECD). *J Cereb Blood Flow Metab* 14(Suppl 1):S4–11

Watanabe M, Okada H, Shimizu K, Omura T, Yoshikawa E, Kosugi T *et al* (1997) A high resolution animal PET scanner using compact PS-PMT detectors. *IEEE Trans Nucl Sci* 44:1277–82

Young AR, Sette G, Touzani O, Rioux P, Derlon JM, MacKenzie ET *et al* (1996) Relationships between high oxygen extraction fraction in the acute stage and final infarction in reversible middle cerebral artery occlusion: an investigation in anesthetized baboons with positron emission tomography. *J Cereb Blood Flow Metab* 16:1176–88

Zhao W, Belayev L, Ginsberg MD (1997) Transient middle cerebral artery occlusion by intraluminal suture: II. Neurological deficits, and pixel-based correlation of histopathology with local blood flow and glucose utilization. *J Cereb Blood Flow Metab* 17:1281–90

Widespread Decrease of Nicotinic Acetylcholine Receptors in Parkinson's Disease

Masahiro Fujita, MD, PhD,[1] Masanori Ichise, MD,[1] Sami S. Zoghbi, PhD,[1] Jeih-San Liow, PhD,[1] Subroto Ghose, MD, PhD,[1] Douglass C. Vines, BS,[1] Janet Sangare, C-RNP, MS,[1] Jian-Qiang Lu, MD, PhD,[1] Vanessa L. Cropley, BS,[1] Hidehiro Iida, PhD,[2] Kyeong Min Kim, PhD,[2] Robert M. Cohen, PhD, MD,[3] William Bara-Jimenez, MD,[4] Bernard Ravina, MD,[5] and Robert B. Innis, MD, PhD[1]

Objective: **Nicotinic acetylcholine receptors have close interactions with the dopaminergic system and play critical roles in cognitive function. The purpose of this study was to compare these receptors between living PD patients and healthy subjects.** *Methods:* **Nicotinic acetylcholine receptors were imaged in 10 nondemented Parkinson's disease patients and 15 age-matched healthy subjects using a single-photon emission computed tomography ligand [^{123}I]5-iodo-3-[2(*S*)-2-azetidinylmethoxy]pyridine. Using an arterial input function, we measured the total distribution volume (V_T; specific plus nondisplaceable), as well as the delivery (K_1).** *Results:* **Parkinson's disease showed a widespread significant decrease (approximately 10%) of V_T in both cortical and subcortical regions without a significant change in K_1.** *Interpretation:* **These results indicate the importance of extending the study to demented patients.**

Ann Neurol 2006;59:174–177

In addition to the well-documented loss of dopaminergic neurons, a number of animal and clinical studies have shown that nicotinic acetylcholine receptors (nAChRs) play critical roles in Parkinson's disease (PD). nAChR activation stimulates dopamine release in the striatum,[1] and an agonist at nAChRs showed synergistic therapeutic effects with L-dopa in a monkey model of PD.[2] Epidemiological studies showed that cigarette smoking protects against PD.[3] Both animal and human studies have shown that nAChR is one of the central components in cognitive function,[4] and a substantial number of PD patients become demented. Finally, most postmortem studies showed widespread decrease of nAChRs both in striatum and cerebral cortices of PD patients.[5–8] However, as in most other postmortem studies, many of these lacked critical clinical information such as the presence of dementia and a history of cigarette smoking. Therefore, it is critical to image nAChRs in living PD patients whose clinical information is available to study changes and to explore possible therapeutic intervention at these receptors. However, to our knowledge, such a study has not been published.

Recently, 3-[2(*S*)-2-azetidinylmethoxy]pyridine (A-85380) has been developed,[9] which has high affinity to the predominant type of nAChRs in the brain composed of α_4 and β_2 subunits.[10] A few analogs of A-85380, including [^{123}I]5-iodo-3-[2(*S*)-2-azetidinylmethoxy]pyridine (5-I-A-85380), have been radiolabeled and used successfully in humans.[11,12] An ex vivo study in nonhuman primate has shown that radiolabeled metabolites of [^{123}I] 5-I-A-85380 do not cross the blood–brain barrier.[13] 5-I-A-85380 labels several β_2-containing nAChRs, including $\alpha_4\beta_2$- (the most predominant nicotinic receptor in human brain), $\alpha_3\beta_2$-, and $\alpha6\beta2$-containing subtypes.[14]

The purpose of this study was to perform a pilot study of nAChR imaging using [^{123}I]5-I-A-85380 in early to moderate stage PD patients.

Subjects and Methods

Subjects

The study was approved by National Institute of Neurological Disorders and Stroke and National Institute of Mental Health institutional review boards. Patients were recruited from National Institute of Neurological Disorders and Stroke clinics. Control subjects were healthy volunteers recruited from community via advertisement who did not have a history or signs of neurological disorders. After complete description of the study to the subjects, written informed consent was obtained. Sample demographics and clinical characteristics are shown in Table 1. For all participants, the absence of axial focal lesions was confirmed by a neuroradiologist using noncontrast magnetic resonance imaging. All patients and healthy subjects had not smoked cigarettes for at least 5 years. None of the patients had used cholinergic or anticholinergic medications within 60 days of the single-photon emission computed tomography (SPECT) scan. On the day of the SPECT scans, all patients continued dopaminergic medications including carbidopa/L-dopa. There was no significant difference in age between PD patients and healthy subjects.

From the [1]Molecular Imaging Branch, National Institute of Mental Health, National Institutes of Health, Bethesda, MD; [2]Investigative Radiology, National Cardiovascular Center Research Institute, Suita, Osaka, Japan; [3]Geriatric Psychiatry Branch, National Institute of Mental Health; [4]Experimental Therapeutics Branch, National Institute of Neurological Disorders and Stroke; and [5]Clinical Trials, Extramural Research, National Institute of Neurological Disorders and Stroke, National Institutes of Health, Bethesda, MD.

Received May 15, 2005, and in revised form Jun 24. Accepted for publication Jun 30, 2005.

Published online Dec 27, 2005 in Wiley InterScience (www.interscience.wiley.com) DOI: 10.1002/ana.20688

Address correspondence to Dr Fujita, Molecular Imaging Branch, National Institute of Mental Health, Building 1, Room B3-10, 1 Center Drive, MSC-0135, Bethesda, MD. E-mail: fujitam@intra.nimh.nih.gov

Table 1. Sample Demographics and Clinical Characteristics

Characteristics	Healthy	PD
N	15	10
Mean age (±SD), yr	59 ± 5	56 ± 3
Sex, F/M	10/5	4/6
Cigarette smoking	No	No
Cholinergic medication	No	No
Dopaminergic medication	No	Yes
Mean [^{123}I]5-I-A-85380 dose (±SD), MBq	486 ± 79	506 ± 75
Mean Hoehn and Yahr staging (±SD)		2.5 ± 0.4
Mean total Unified Parkinson's Disease Rating Scale score (±SD)		46 ± 5[a]
Mean Mini-Mental Status Examination score		≥27
Mean Mattis Dementia Rating Scale score (±SD)		135 ± 4[b]

[a]N = 9; [b]N = 8.

PD = Parkinson's disease; SD = standard deviation.

Clinical Ratings

Motor function was evaluated by Unified Parkinson's Disease Rating Scale and Hoehn and Yahr staging. Cognitive function was measured with Mini-Mental Status Examination and Mattis Dementia Rating Scale.

Single-Photon Emission Computed Tomography

[^{123}I]5-I-A-85380 was prepared as described previously.[12] SPECT data were acquired using a triple-headed camera with low-energy, high-resolution, parallel hole collimators (Trionix XLT-20; Triad, Twinsburg, OH). Initially, a transmission scan was obtained using a ^{153}Gd line source. Subsequently, [^{123}I]5-I-A-85380 was administered intravenously as a bolus (injection dose: healthy, 486 ± 79MBq; PD, 506 ± 75MBq; no significant difference, with these and subsequent data expressed as mean ± standard deviation). SPECT data were acquired at 0 to 40, 115 to 135, and 210 to 230 minutes. Arterial samples were obtained every 15 seconds for the first 2 minutes and at 3, 4, 5, 10, 30, 80, 120, and 180 minutes.

Plasma Analysis

Plasma [^{123}I]5-I-A-85380 concentration and the free fraction (f_1) were determined as described previously.[12]

Image Analysis

SPECT projection data were reconstructed on a 64 × 64 matrix with pixel size of 4.48 × 4.48 × 4.48mm in the *x*-, *y*-, and *z*-axis, respectively, with correction for attenuation and scattered radiation.[15] Parametric images of the delivery of the radioligand (K_1) and total distribution volume (V) were created using a multilinear algorithm[16,17] implemented in PMOD 2.55 (http://www.pmod.com/technologies/index.html). Plasma free [^{123}I]5-I-A-85380 levels were used to calculate V instead of using plasma total (free plus protein bound) [^{123}I]5-I-A-85380 because patients were taking medication and concomitant medication might change plasma protein binding of [^{123}I]5-I-A-85380. Parametric images were spatially normalized to a standard anatomic orientation (Montreal Neurological Institute space) based on K_1 images and using Statistical Parametric Mapping version '02 (SPM2; http://www.fil.ion.ucl.ac.uk/spm). Spatially normalized K_1 and V images were smoothed with 10mm full-width at half-maximum. To confirm the magnitude of changes in V, we obtained volume of interest data from brain regions in Montreal Neurological Institute space listed on Table 2.

Statistical Analysis

SPM2[18] was used for statistical analysis. Two-sample *t* test was applied to compare K_1 and V between patients and healthy subjects, and simple regression analysis was applied to study the relationship between V and clinical ratings. Gray matter threshold was set at 20% for V and 80% for K_1 images, respectively. Because each pixel had a measured value of K_1 or V, global normalization was not applied. No sphericity correction was applied by assuming replication over groups. False-discovery rate of p less than 0.05 and cluster-level corrected p less than 0.05 were considered significant.

A two-sample *t* test was applied to compare plasma free fraction of [^{123}I]5-I-A-85380 between groups.

Results

Patients were in the early to moderate stages of PD and were not demented (see Table 1). Patients tended to show lower f_1 values than healthy subjects (p = 0.09; see Table 2).

An SPM *t* test showed a significant decrease of V in many brain regions with the greatest T value of 4.96 (Fig). The decrease measured by the volume of interest was 15% in thalamus, whereas occipital and frontal cortices showed only 3 and 5% decreases, respectively, where many voxels did not reach significance. Decreases in parietal and temporal cortices were 8 to 9% (see Table 2). SPM did not detect a significant increase of V in any brain region in patients. There was neither a significant increase nor a decrease of K_1 in any re-

Table 2. Plasma-Free Fraction and Total Distribution Volume of [^{123}I]5-I-A-85380

Measurements	Healthy	PD
Plasma-free fraction, %	48.1 ± 4.4	45.3 ± 3.1
Total distribution volume, ml/cm^3		
Thalamus	71.9 ± 13.5	61.2 ± 10.7
Caudate	41.9 ± 6.2	36.9 ± 4.3
Putamen	44.4 ± 6.7	40.2 ± 5.6
Pons	43.3 ± 8.1	39.0 ± 8.1
Frontal cortex	24.9 ± 3.1	23.7 ± 3.1
Parietal cortex	26.9 ± 3.5	24.4 ± 3.0
Temporal cortex	30.7 ± 3.9	28.1 ± 4.0
Occipital cortex	27.1 ± 3.6	26.3 ± 4.2
Cerebellum	33.8 ± 6.2	29.2 ± 5.9[a]

[a]One patient was excluded whose cerebellum was partially out of field of view

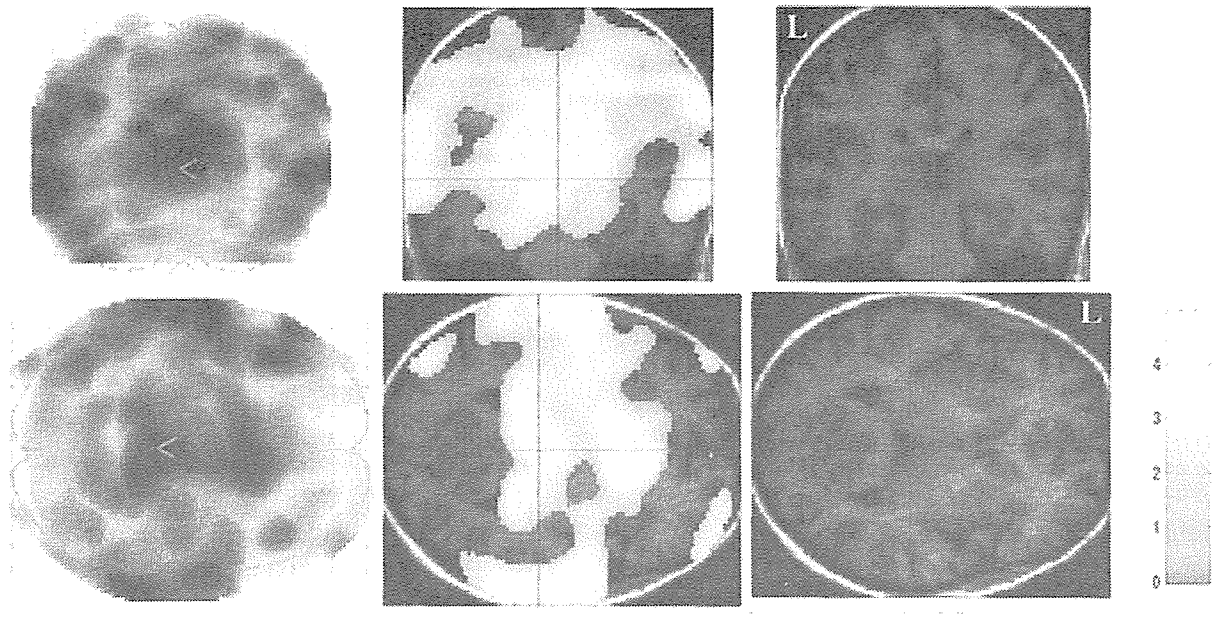

Fig. Brain areas with a significant decrease of [^{123}I]5-I-A-85380 distribution volume (V) *in Parkinson's disease patients detected with a two-sample* t *test in Statistical Parametric Mapping version '02. Areas with a significant decrease are displayed in the glass brain (left) and on transverse and coronal slices through thalamus of a magnetic resonance (MR) image of a control subject (middle). Corresponding MR images without superimposition are shown on the right. Highlighted areas showed* p *less than 0.05 false-discovery rate, which was corrected for multiple comparisons. The area also showed cluster-level corrected* p *less than 0.001. Color bar shows* T *values with the maximum value of 4.96. Note that the glass brain view displays decreases in the entire brain superimposed to anteroposterior (top left) or top-bottom (bottom left) views, whereas the MR images with the superimposition display decreases on single slices.*

gion. There was no significant regression between any clinical rating scores and *V*.

Discussion

In this study, we detected a significant and widespread decrease of nAChRs in early to moderately affected, nondemented PD patients by applying accurate quantification with the measurement of arterial input function and the plasma free fraction (f_1) of [^{123}I]5-I-A-85380 in each subject. Such measurements made the outcome of imaging studies free from intersubject and between-group differences in the metabolism and the protein binding of the imaging agent. Because patients tended to show lower f_1 values, if total plasma parent had been used instead of free [^{123}I]5-I-A-85380, the decrease in *V* would have been overestimated. Furthermore, for accurate measurement, scatter correction[15] and a pixel-based modeling that minimizes noise-induced biases[16,17] were applied.

There are three possible reasons that the decreases in *V* detected in this study were smaller than those reported at postmortem (>30% in most studies). First, because there is no large region devoid of nAChRs, it was not possible to measure nondisplaceable radioactivity, which then could have been used to calculate specific binding of [^{123}I]5-I-A-85380. Because *V* is a summation of specific and nondisplaceable distribution volumes, a decrease of specific binding was underestimated. Second, in this pilot study, only nondemented PD patients were enrolled, whereas postmortem studies found larger decreases in nAChRs in demented patients.[5,7] Therefore, postmortem studies including demented patients showed greater decreases in nAChR than in this study. The lack of significant regression between clinical ratings and *V* may also be explained by a fairly uniform population of nondemented patients. Third, whereas B_{max} is measured in postmortem studies, B_{max}/K_d plus nondisplaceable activity is measured by *in vivo* imaging studies including this one. If there were a decrease in K_d measured *in vivo* in addition to a decrease in B_{max}, a decrease in B_{max}/K_d would not be as great as that in B_{max}. In fact, a postmortem study reported a nonsignificant but substantial 10 to 40% decrease in K_d in both cortical and subcortical regions.[6]

There are a couple of factors that may confound interpretation of the results of this study. All patients were taking L-dopa–containing medications. L-Dopa treatment significantly decreased *in vitro* [^{125}I]5-I-A-85380 binding in the striatum, but not in cerebral cortex in normal squirrel monkeys.[19] However, in the same study, L-dopa treatment did not decrease [^{125}I]5-I-A-85380

binding in the same regions in 1-methyl-4-phenyl-1,2,3,6-tetrahydropyridine–treated animals whose dopaminergic terminals were almost completely destroyed. Therefore, the widespread decreases in nAChRs found in this study are more likely to be the result of PD pathology than L-dopa treatment. Brain atrophy can cause widespread decrease in nAChRs detected in SPECT. However, a voxel-based morphometric study on nondemented patients did not detect a widespread decrease in gray matter volume.[20] By taking together the factors described earlier, nondemented patients with PD did show a widespread decrease of B_{max}/K_d in β_2-containing nAChRs both in cortices and subcortical regions. Because postmortem studies have shown greater decreases in nAChRs in demented patients, it would be interesting to extend the study to include such patients.

This study was supported by the NIH (Intramural Program, 2D1MH002796-04, R.B.I.).

We thank Dr C. Chen and the National Institutes of Health Nuclear Medicine Department for providing the SPECT camera for this study; Drs C. Burger, P. Rudnicki, K. Mikolajczyk, M. Grodzki, and M. Szabatin for providing PMOD 2.55; and A. Crawley, J. Szczepanik, and M. Gillespie for subject recruitment.

References

1. Rapier C, Lunt GG, Wonnacott S. Stereoselective nicotine-induced release of dopamine from striatal synaptosomes: concentration dependence and repetitive stimulation. J Neurochem 1988;50:1123–1130.
2. Schneider JS, Pope-Coleman A, Van Velson M, et al. Effects of SIB-1508Y, a novel neuronal nicotinic acetylcholine receptor agonist, on motor behavior in parkinsonian monkeys. Mov Disord 1998;13:637–642.
3. Tanner CM, Goldman SM, Aston DA, et al. Smoking and Parkinson's disease in twins. Neurology 2002;58:581–588.
4. Picciotto MR, Zoli M. Nicotinic receptors in aging and dementia. J Neurobiol 2002;53:641–655.
5. Rinne JO, Myllykyla T, Lonnberg P, Marjamaki P. A postmortem study of brain nicotinic receptors in Parkinson's and Alzheimer's disease. Brain Res 1991;547:167–170.
6. Aubert I, Araujo DM, Cecyre D, et al. Comparative alterations of nicotinic and muscarinic binding sites in Alzheimer's and Parkinson's diseases. J Neurochem 1992;58:529–541.
7. Lange KW, Wells FR, Jenner P, Marsden CD. Altered muscarinic and nicotinic receptor densities in cortical and subcortical brain regions in Parkinson's disease. J Neurochem 1993;60:197–203.
8. Quik M, Bordia T, Forno L, McIntosh JM. Loss of alpha-conotoxinMII- and A85380-sensitive nicotinic receptors in Parkinson's disease striatum. J Neurochem 2004;88:668–679.
9. Abreo MA, Lin NH, Garvey DS, et al. Novel 3-pyridyl ethers with subnanomolar affinity for central neuronal nicotinic acetylcholine receptors. J Med Chem 1996;39:817–825.
10. Mukhin AG, Gundisch D, Horti AG, et al. 5-Iodo-A-85380, an a4b2 subtype-selective ligand for nicotinic acetylcholine receptors. Mol Pharmacol 2000;57:642–649.
11. Sihver W, Nordberg A, Langstrom B, et al. Development of ligands for in vivo imaging of cerebral nicotinic receptors. Behav Brain Res 2000;113:143–157.
12. Fujita M, Ichise M, van Dyck CH, et al. Quantification of nicotinic acetylcholine receptors in human brain using [^{123}I]5-I-A-85380 SPET. Eur J Nucl Med 2003;30:1620–1629.
13. Baldwin RM, Zoghbi SS, Staley JK, et al. Chemical composition of ^{123}I-5-IA in baboon brain after intravenous administration. J Nucl Med 2002;43:45P.
14. Kulak JM, Sum J, Musachio JL, et al. 5-Iodo-A-85380 binds to alpha-conotoxin MII-sensitive nicotinic acetylcholine receptors (nAChRs) as well as alpha4beta2* subtypes. J Neurochem 2002;81:403–406.
15. Iida H, Narita Y, Kado H, et al. Effects of scatter and attenuation correction on quantitative assessment of regional cerebral blood flow with SPECT. J Nucl Med 1998;39:181–189.
16. Ichise M, Toyama H, Innis RB, Carson RE. Strategies to improve neuroreceptor parameter estimation by linear regression analysis. J Cereb Blood Flow Metab 2002;22:1271–1281.
17. Ichise M, Fujita M, Zoghbi SS, et al. Parametric imaging of distribution volume and tracer delivery by noise-resistant linear regression analysis: application to [^{123}I]5-I-A-85380 SPECT imaging of a4b2 nicotinic acetylcholine receptors in human. NeuroImage 2004;22:T180–T181.
18. Friston KJ, Holmes AP, Worsley KJ, et al. Statistical parametric maps in functional imaging: a general linear approach. Hum Brain Mapping 1995;2:189–210.
19. Quik M, Bordia T, Okihara M, et al. L-DOPA treatment modulates nicotinic receptors in monkey striatum. Mol Pharmacol 2003;64:619–628.
20. Burton EJ, McKeith IG, Burn DJ, et al. Cerebral atrophy in Parkinson's disease with and without dementia: a comparison with Alzheimer's disease, dementia with Lewy bodies and controls.Brain 2004;127:791–800.

Japanese Journal of Applied Physics
Vol. 45, No. 10A, 2006, pp. 8005–8009

Enhanced Magnification Angiography Using 20-μm-Focus Tungsten Tube

Toshiyuki ENOMOTO, Eiichi SATO[1], Yoshinobu SUMIYAMA, Katsuo AIZAWA[2], Manabu WATANABE, Etsuro TANAKA[3], Hidezo MORI[4], Hiroki KAWAKAMI[5], Toshiaki KAWAI[5], Takashi INOUE[6], Akira OGAWA[6] and Shigehiro SATO[7]

The 3rd Department of Surgery, Toho University School of Medicine, 2-17-6 Ohashi, Meguro-ku, Tokyo 153-8515, Japan
[1]*Department of Physics, Iwate Medical University, 3-16-1 Honchodori, Morioka 020-0015, Japan*
[2]*Tokyo Medical University [emeritus professor], 6-1-1 Shinjuku, Shinjuku-ku, Tokyo 160-8402, Japan*
[3]*Department of Nutritional Science, Faculty of Applied Bio-science, Tokyo University of Agriculture, 1-1-1 Sakuragaoka, Setagaya-ku, Tokyo 156-8502, Japan*
[4]*Department of Cardiac Physiology, National Cardiovascular Center Research Institute, 5-7-1 Fujishirodai, Suita, Osaka 565-8565, Japan*
[5]*Electron Tube Division #2, Hamamatsu Photonics K.K., 314-5 Shimokanzo, Iwata, Shizuoka 438-0193, Japan*
[6]*Department of Neurosurgery, School of Medicine, Iwate Medical University, 19-1 Uchimaru, Morioka 020-8505, Japan*
[7]*Department of Microbiology, School of Medicine, Iwate Medical University, 19-1 Uchimaru, Morioka 020-8505, Japan*

(Received April 10, 2006; accepted June 25, 2006; published online October 6, 2006)

A microfocus X-ray tube is useful for performing magnification radiography, and its X-ray generator (L9631, Hamamatsu Photonics) consists of a personal computer for controlling the tube voltage and current, and a main unit with a high-voltage circuit and a fixed-anode X-ray tube. The maximum tube voltage, current, and electric power were 110 kV, 800 μA, and 50 W, respectively. The focal-spot size was proportional to the electric power of the tube, and the size was approximately 20 μm with a power of 20 W. Using a 3-mm-thick aluminum filter, the X-ray intensity was 7.75 μGy/s at 1.0 m from the source with a tube voltage of 60 kV and a current of 100 μA. Because the peak photon energy was approximately 38 keV using the filter with a tube voltage of 60 kV, the bremsstrahlung X-rays were absorbed effectively by iodine-based contrast media at an iodine K-edge of 33.2 keV. Enhanced angiography was performed by fourfold magnification imaging with a computed radiography system using iodine-based microspheres 15 μm in diameter. In the angiography of nonliving animals, we observed fine blood vessels of approximately 100 μm with high contrast. [DOI: 10.1143/JJAP.45.8005]

KEYWORDS: high-contrast angiography, magnification digital radiography, microfocus X-ray tube, energy-selective imaging

1. Introduction

To perform high-speed medical radiography, several various flash X-ray generators using cold-cathode tubes have been developed.[1–4] In particular, quasi-monochromatic flash X-ray generators[5–10] have been designed to perform preliminary experiments for producing clean K-series X-rays, and higher-harmonic hard X-rays have been observed in a weakly ionized linear plasma of copper and nickel. However, in monochromatic flash radiography, difficulties in increasing X-ray duration and in performing X-ray computed tomography (CT) have been encountered.

Synchrotrons are capable of producing high-dose-rate monochromatic parallel X-ray beams using silicon crystals, and the beams have been applied to phase-contrast radiography[11,12] and enhanced K-edge angiography.[13,14] In angiography, monochromatic X-rays with photon energies ranging from 33.3 to 35 keV have been employed because the rays are absorbed effectively by iodine-based contrast media with an iodine K-edge of 33.2 keV.

Without using synchrotrons, phase-contrast radiography[15] for edge enhancement can be performed using a microfocus X-ray tube, and the enhancement has been achieved in mammography[16] with a computed radiography (CR) system[17] using a 100-μm-focus tube. Subsequently, we developed a cerium X-ray generator[18,19] to perform enhanced K-edge angiography using cone beams, and succeeded in observing fine blood vessels and coronary arteries with high contrast using cerium Kα-rays of 34.6 keV.

Although the magnification radiography is used to improve the spatial resolution in angiography utilizing a digital imaging system, it is difficult to design a small focus cerium tube for angiography. Therefore, narrow-photon-energy bremsstrahlung X-rays[20–22] with a peak energy of approximately 35 keV from a tungsten tube are used to perform high-contrast angiography.

In this research, we employed a microfocus tungsten tube, and performed enhanced magnification angiography by controlling bremsstrahlung X-ray spectra using an aluminum filter.

2. Principle of Enhanced Magnification Angiography

Figure 1 shows the mass attenuation coefficients of iodine at the selected energies; the coefficient curve is discontinuous at the iodine K-absorption edge of 33.2 keV. The effective bremsstrahlung X-rays for K-edge angiography are shown above the K-edge. Using a 3.0-mm-thick aluminum filter for absorbing soft X-rays, the peak photon energy of the bremsstrahlung rays increases to approximately 38 keV. In angiography, iodine contrast media in blood vessels easily absorb the rays, and soft bremsstrahlung rays are absorbed effectively by objects (muscles). Therefore, blood vessels are observed with high contrast. Subsequently, spatial resolution is improved by fourfold magnification imaging using a microfocus X-ray tube in conjunction with a CR system (Regius 150, Konica Minolta) at a sampling pitch of 87.5 μm.

3. Experimental Methods

The microfocus X-ray generator (L9631, Hamamatsu Photonics) consists of a personal computer and a system unit. The unit includes all the hardware in the X-ray generator, such as, a high-voltage circuit and a fixed anode X-ray tube. Tube voltage, current, and exposure time can be controlled by the computer. The maximum tube voltage, current, and electric power were 110 kV, 800 μA, and 50 W,

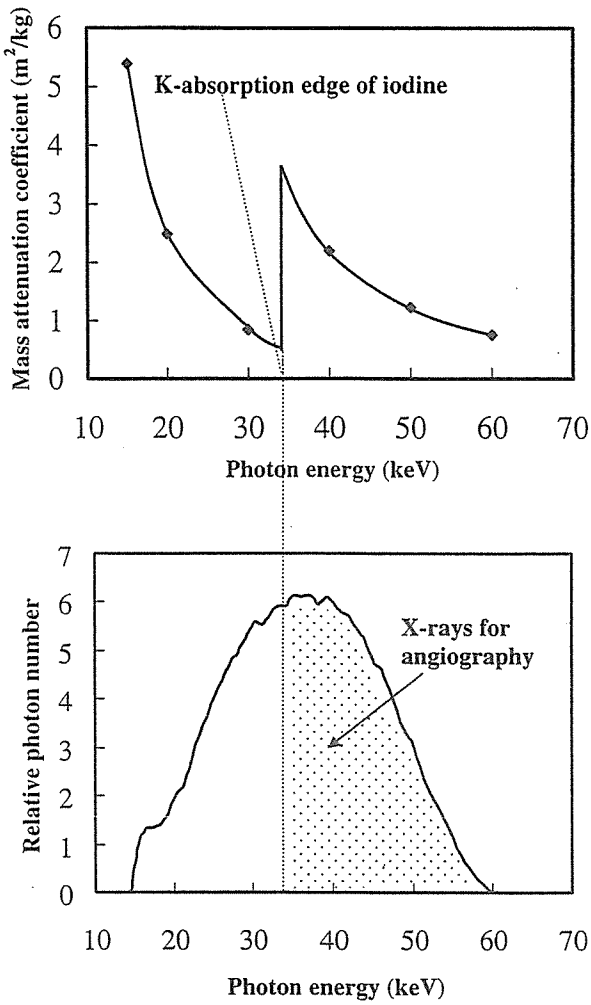

Fig. 1. Mass attenuation coefficients of iodine and bremsstrahlung X-rays for enhanced K-edge angiography.

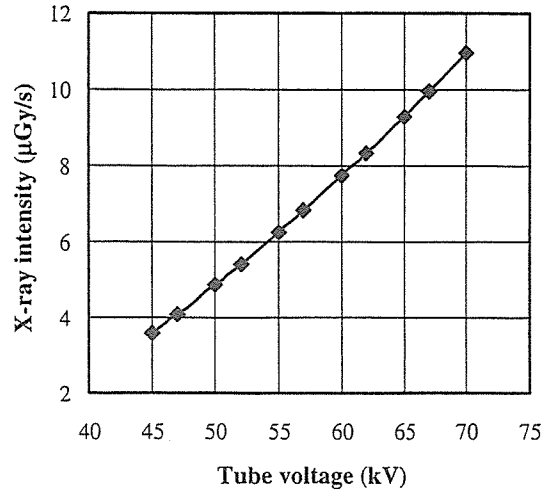

Fig. 2. X-ray intensity (μGy/s) as a function of tube voltage (kV) with tube current of 100 μA.

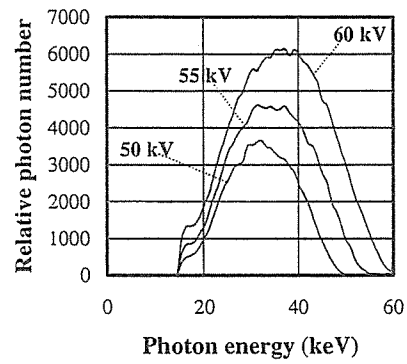

Fig. 3. Bremsstrahlung X-ray spectra measured using cadmium telluride detector with changes in tube voltage.

respectively. The focal-spot size was proportional to the electric power of the tube, and its size was approximately 20 μm in diameter with a power of 20 W. In this experiment, the tube voltage applied ranged from 45 to 70 kV, and the tube current was regulated to within 170 μA. The exposure time is controlled to obtain optimum X-ray intensity for angiography, and narrow-photon-energy bremsstrahlung X-rays are produced using the aluminum filter.

4. Results

4.1 X-ray intensity

X-ray intensity was measured using a Victoreen 660 ionization chamber, with a volume of 400 cm^3, at 1.0 m from the X-ray source using the filter (Fig. 2). At a constant tube current of 100 μA, X-ray intensity increased when tube voltage was increased. At a tube voltage of 60 kV, the X-ray intensity with the filter was 7.75 μGy/s.

4.2 X-ray spectra

To measure X-ray spectra using the filter, we employed a cadmium telluride detector (CDTE2020X, Hamamatsu Photonics) (Fig. 3). When tube voltage was increased, bremsstrahlung X-ray intensity increased, and both maximum photon energy and spectrum peak energy increased.

To perform K-edge angiography, bremsstrahlung X-rays of approximately 35 keV are used; the high-energy bremsstrahlung X-rays decrease image contrast. When this filter was used, because bremsstrahlung X-rays with energies higher than 60 keV were not absorbed easily, the tube voltage for angiography was determined to be 60 kV by considering the filtering effect of radiographic objects.

4.3 Enhanced magnification angiography

The enhanced angiography was performed by fourfold magnification imaging using the CR system and the filter at a tube voltage of 60 kV, and the distance between the X-ray source and the imaging plate was 1.0 m (Fig. 4). First, the spatial resolutions of cohesion and magnification radiographies were realized using a lead test chart at an exposure time of 30 s. In the magnification radiography, 50-μm-thick lines (10 line pairs) were clearly visible (Fig. 5). Figure 6 shows radiograms of tungsten wires in a 25-mm-diameter rod made of poly(methyl methacrylate) (PMMA) at an exposure time of 30 s. Although image contrast decreased slightly with decreasing wire diameter owing to the blurring of the image caused by the sampling pitch of 87.5 μm, a 20-μm-diameter wire could be observed.

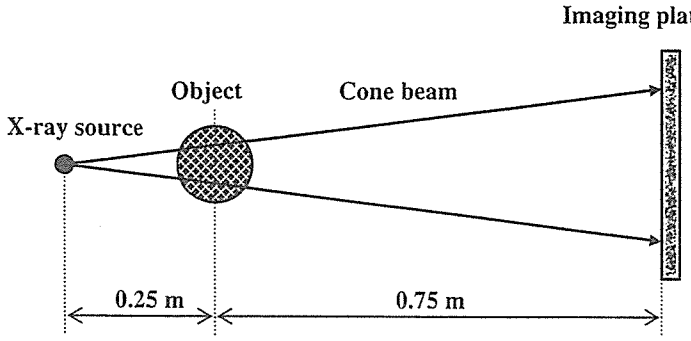

Fig. 4. Fourfold magnification imaging using imaging plate in conjunction with microfocus tube.

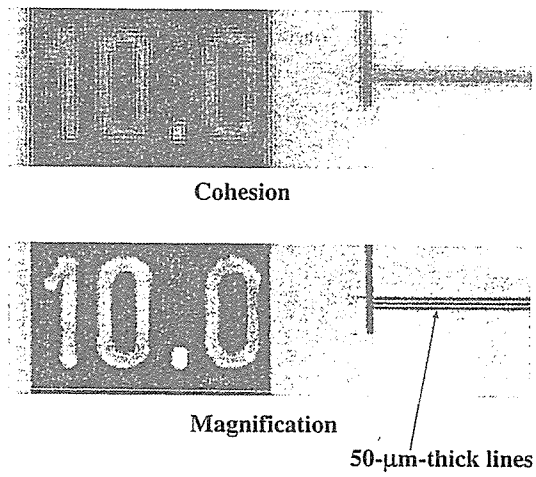

Fig. 5. Radiogram of test chart for measuring spatial resolution.

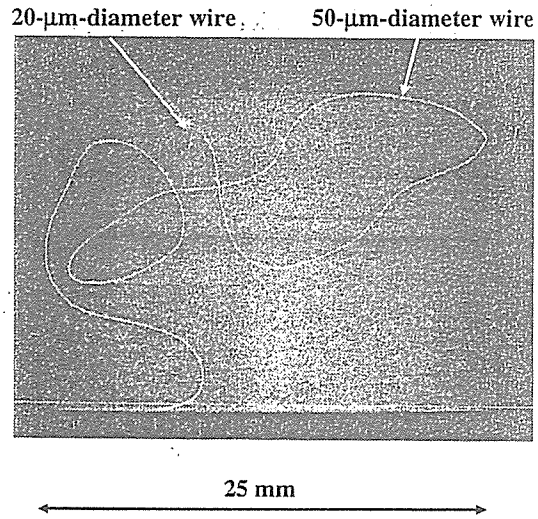

Fig. 6. Radiograms of tungsten wires in PMMA rod.

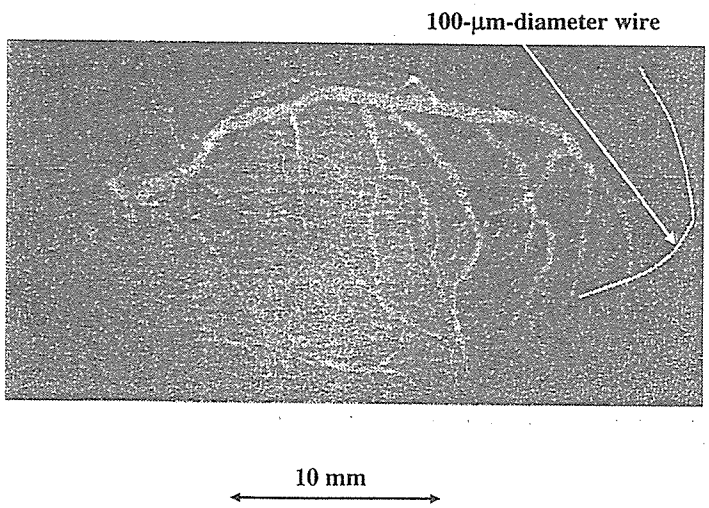

Fig. 7. Angiogram of extracted rabbit heart using iodine microspheres.

Figures 7 and 8 show angiograms of a 19-mm-thick rabbit heart specimen and a 41-mm-thick thigh specimen, respectively. The exposure time was 30 s, and these images were obtained using iodine microspheres of 15 μm diameter. The microspheres are very useful for making the phantoms of nonliving animals used for angiography. The iodine plastic spheres contained 37% iodine by weight, and the coronary arteries and fine blood vessels were visible.

Figure 9 shows angiograms of a dog heart specimen of 65 mm thickness using iodine spheres with an exposure time of 60 s. Although the image contrast decreased slightly with increasing thickness of the PMMA plate facing the X-ray

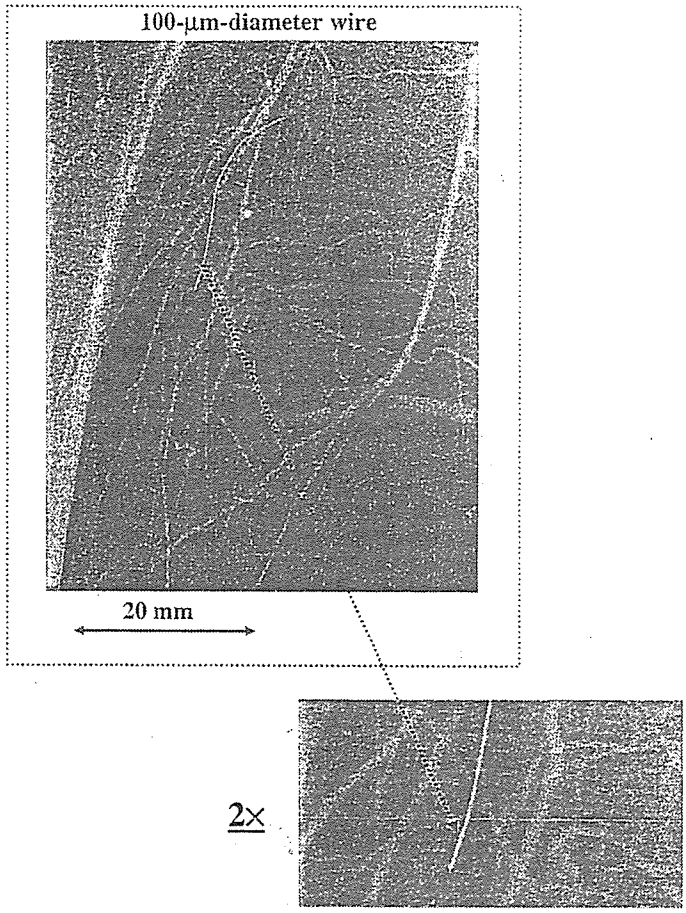

Fig. 8. Angiograms of rabbit thigh.

source, the coronary arteries of approximately 100 μm diameter were observed using a 100-mm-thick plate.

5. Conclusions

We employed a microfocus X-ray generator with a tungsten target tube to perform enhanced magnification angiography using narrow-photon-energy bremsstrahlung X-rays at a peak photon energy of approximately 38 keV, which can be absorbed easily by iodine-based contrast media. Although bremsstrahlung X-ray intensity substantially increased with increasing tube voltage, the optimal tube voltage for increasing image contrast was determined to be 60 kV.

Because the sampling pitch of the CR system is 87.5 μm, we obtained spatial resolutions of approximately 50 μm using fourfold magnification imaging achieved with a 20-μm-focus tube. To observe fine blood vessels of less than 100 μm diameter, the spatial resolution of the CR system should be improved to 43.8 μm (Regius 190, Konica Minolta), and iodine density should be increased.

In this research, we controlled bremsstrahlung X-rays to the optimum spectral distribution for realizing enhanced angiography using iodine-based contrast media. On the other hand, gadolinium-based contrast media with a K-edge energy of 50.2 keV have been employed to perform angiography in MRI, and the gadolinium density used has been increasing. In view of this situation, tungsten Kα rays (58.9 keV) are useful for enhancing K-edge angiography, because the Kα rays are absorbed effectively by gadolinium media. As compared with angiography using iodine media, the absorbed dose can be decreased considerably using gadolinium media.

At a tube voltage of 60 kV and a current of 170 μA, the photon number was approximately 2×10^7 photons/(cm^2·s) at 1.0 m from the source, and photon count rate can be increased easily using a rotating anode microfocus tube developed by Hitachi Medical Corporation. Recently, the maximum electric power of the microfocus X-ray tube has been increasing, and a kilowatt-range tube is realizable. Therefore, real-time magnification radiography will become possible using a flat panel detector with a pixel size of less than 100 μm.

Acknowledgments

This work was supported by Grants-in-Aid for Scientific Research (13470154, 13877114, and 16591222) and Advanced Medical Scientific Research from MECSST, Health and Labor Sciences Research Grants (RAMT-nano-001, RHGTEFB-genome-005 and RHGTEFB-saisei-003), and grants from the Keiryo Research Foundation, Promotion and Mutual Aid Corporation for Private Schools of Japan, Japan Science and Technology Agency (JST), and New Energy and Industrial Technology Development Organization (NEDO, Industrial Technology Research Grant Program in '03).

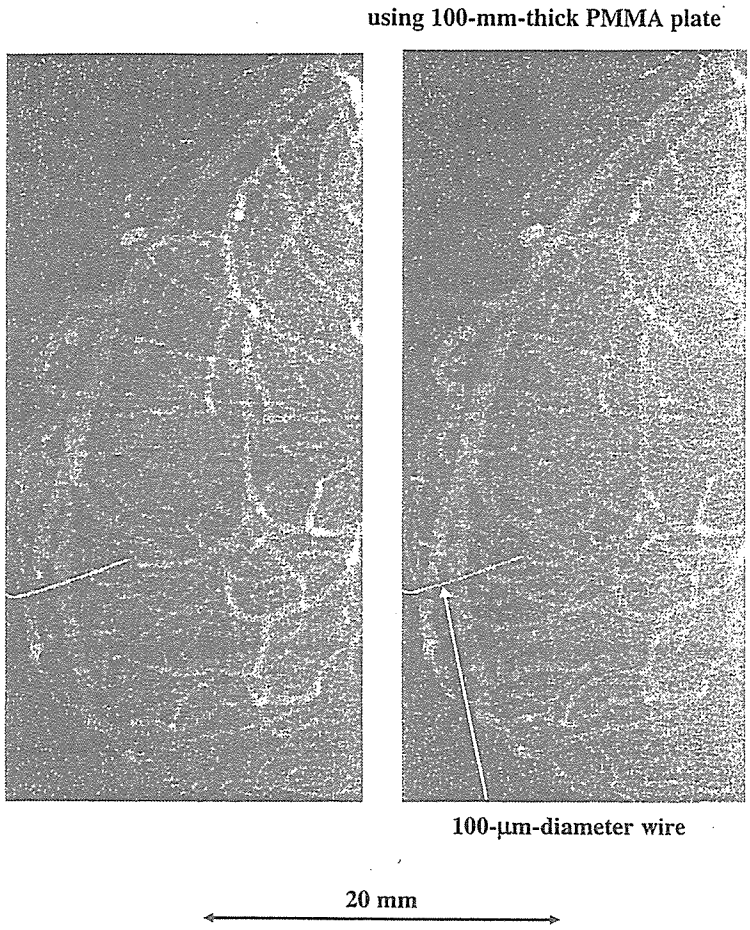

Fig. 9. Angiograms of extracted dog heart.

1) E. Sato, S. Kimura, S. Kawasaki, H. Isobe, K. Takahashi, Y. Tamakawa and T. Yanagisawa: Rev. Sci. Instrum. **61** (1990) 2343.
2) K. Takahashi, E. Sato, M. Sagae, T. Oizumi, Y. Tamakawa and T. Yanagisawa: Jpn. J. Appl. Phys. **33** (1994) 4146.
3) E. Sato, K. Takahashi, M. Sagae, S. Kimura, T. Oizumi, Y. Hayasi, Y. Tamakawa and T. Yanagisawa: Med. Biol. Eng. Comput. **32** (1994) 289.
4) E. Sato, M. Sagae, K. Takahashi, A. Shikoda, T. Oizumi, Y. Hayasi, Y. Tamakawa and T. Yanagisawa: Med. Biol. Eng. Comput. **32** (1994) 295.
5) E. Sato, Y. Hayasi, R. Germer, E. Tanaka, H. Mori, T. Kawai, T. Ichimaru, K. Takayama and H. Ido: Rev. Sci. Instrum. **74** (2003) 5236.
6) E. Sato, Y. Hayasi, R. Germer, E. Tanaka, H. Mori, T. Kawai, T. Ichimaru, S. Sato, K. Takayama and H. Ido: J. Electron Spectrosc. Relat. Phenom. **137–140** (2004) 713.
7) E. Sato, E. Tanaka, H. Mori, T. Kawai, S. Sato and K. Takayama: Opt. Eng. **44** (2005) 049002.
8) E. Sato, M. Sagae, E. Tanaka, Y. Hayasi, R. Germer, H. Mori, T. Kawai, T. Ichimaru, S. Sato, K. Takayama and H. Ido: Jpn. J. Appl. Phys. **43** (2004) 7324.
9) E. Sato, E. Tanaka, H. Mori, T. Kawai, T. Ichimaru, S. Sato, K. Takayama and H. Ido: Med. Phys. **32** (2005) 49.
10) E. Sato, Y. Hayasi, K. Kimura, E. Tanaka, H. Mori, T. Kawai, T. Inoue, A. Ogawa, S. Sato, K. Takayama, J. Onagawa and H. Ido: Jpn. J. Appl. Phys. **44** (2005) 8716.
11) A. Momose, T. Takeda, Y. Itai and K. Hirano: Nat. Med. **2** (1996) 473.
12) M. Ando, A. Maksimenko, H. Sugiyama, W. Pattanasiriwisawa, K. Hyodo and C. Uyama: Jpn. J. Appl. Phys. **41** (2002) L1016.
13) H. Mori, K. Hyodo, E. Tanaka, M. U. Mohammed, A. Yamakawa, Y. Shinozaki, H. Nakazawa, Y. Tanaka, T. Sekka, Y. Iwata, S. Honda, K. Umetani, H. Ueki, T. Yokoyama, K. Tanioka, M. Kubota, H. Hosaka, N. Ishizawa and M. Ando: Radiology **201** (1996) 173.
14) K. Hyodo, M. Ando, Y. Oku, S. Yamamoto, T. Takeda, Y. Itai, S. Ohtsuka, Y. Sugishita and J. Tada: J. Synchrotron Radiat. **5** (1998) 1123.
15) S. W. Wilkins, T. E. Gureyev, D. Gao, A. Pogany and A. W. Stevenson: Nature **384** (1996) 335.
16) A. Ishisaka, H. Ohara and C. Honda: Opt. Rev. **7** (2000) 566.
17) E. Sato, K. Sato and Y. Tamakawa: Annu. Rep. Iwate Med. Univ. School Liberal Arts Sci. **35** (2000) 13.
18) E. Sato, E. Tanaka, H. Mori, T. Kawai, T. Ichimaru, S. Sato, K. Takayama and H. Ido: Med. Phys. **31** (2004) 3017.
19) E. Sato, E. Tanaka, H. Mori, T. Kawai, T. Inoue, A. Ogawa, A. Yamadera, S. Sato, F. Ito, K. Takayama, J. Onagawa and H. Ido: Jpn. J. Appl. Phys. **44** (2005) 8204.
20) A. B. Crummy, C. A. Mistretta, M. G. Ort, F. Kelcz, J. R. Cameron and M. P. Siedband: Radiology **8** (1973) 402.
21) R. A. Kruger, C. A. Mistretta, A. B. Crummy, J. F. Sackett, M. M. Goodsit, S. J. Riederer, T. L. Houk, C. G. Shaw and D. Flemming: Radiology **125** (1977) 234.
22) F. Kelcz and C. A. Mistretta: Med. Phys. **3** (1977) 159.

Available online at www.sciencedirect.com
ScienceDirect
Biochemical and Biophysical Research Communications 349 (2006) 1242–1249
BBRC
www.elsevier.com/locate/ybbrc

Beraprost sodium enhances neovascularization in ischemic myocardium by mobilizing bone marrow cells in rats

Yoshinori Miyahara [a], Shunsuke Ohnishi [a], Hiroaki Obata [a], Kozo Ishino [b], Shunji Sano [b], Hidezo Mori [c], Kenji Kangawa [d], Soichiro Kitamura [e], Noritoshi Nagaya [a,*]

[a] *Department of Regenerative Medicine and Tissue Engineering, National Cardiovascular Center Research Institute, Osaka, Japan*
[b] *Department of Cardiovascular Surgery, Okayama University Graduate School of Medicine, Dentistry and Pharmaceutical Sciences, Okayama, Japan*
[c] *Department of Cardiac Physiology, National Cardiovascular Center Research Institute, Osaka, Japan*
[d] *Department of Biochemistry, National Cardiovascular Center Research Institute, Osaka, Japan*
[e] *Department of Cardiovascular Surgery, National Cardiovascular Center, Osaka, Japan*

Received 13 August 2006
Available online 7 September 2006

Abstract

Beraprost sodium, an orally active prostacyclin analogue, has vasoprotective effects such as vasodilation and antiplatelet activities. We investigated the therapeutic potential of beraprost for myocardial ischemia. Immediately after coronary ligation of Sprague–Dawley rats, beraprost (200 μg/kg/day) or saline was subcutaneously administered for 28 days. Four weeks after coronary ligation, administration of beraprost increased capillary density in ischemic myocardium, decreased infarct size, and improved cardiac function in rats with myocardial infarction. Beraprost markedly increased the number of CD34-positive cells and c-kit-positive cells in plasma. Also, four weeks after coronary ligation of chimeric rats with GFP-expressing bone marrow, bone marrow-derived cells were incorporated into the infarcted region and its border zone. Treatment with beraprost increased the number of GFP/von Willebrand factor-double-positive cells in the ischemic myocardium. These results suggest that beraprost has beneficial effects on ischemic myocardium partly by its ability to enhance neovascularization in ischemic myocardium by mobilizing bone marrow cells.

Keywords: Prostacyclin analogue; Myocardial infarction; Neovascularization; Bone marrow mobilization

Interruption of myocardial blood flow leads to rapid death of cardiomyocytes and vascular structures, resulting in the development of heart failure [1]. Stem or progenitor cells are mobilized from bone marrow into the peripheral blood in response to tissue ischemia, migrate to sites of injured tissues, and differentiate into endothelial cells and cardiomyocytes [2–4]. However, the compensatory mechanisms are insufficient to heal infarcted myocardium. Earlier studies have shown that bone marrow cells artificially mobilized by cytokines repair the infarcted heart and improve cardiac function after acute myocardial infarction [5,6]. Therefore, enhancement of bone marrow cell mobilization leading to neovascularization following revascularization would be beneficial for the treatment of acute myocardial infarction.

Beraprost sodium (BPS) is a chemically stable prostacyclin analogue owing to its cyclo-pentabenzofuranyl structure [7]. It has been well established that BPS has vasoprotective effects such as vasodilation and antiplatelet activities [8–11]. Thus, BPS has been used in the treatment of peripheral arterial disease [12,13] and pulmonary arterial hypertension [14,15]. Although a limited number of studies suggest therapeutic potential of prostacyclin for the treatment of myocardial ischemia [16–18], the underlying mechanisms still remain unclear. In addition, little information is available regarding the therapeutic potential of prostacyclin analogues such as BPS for myocardial ischemia. A recent study has shown that BPS activates endothelial

* Corresponding author. Fax: +81 6 6833 9865.
E-mail address: nnagaya@ri.ncvc.go.jp (N. Nagaya).

0006-291X/$ - see front matter © 2006 Elsevier Inc. All rights reserved.
doi:10.1016/j.bbrc.2006.08.178

nitric oxide synthase (eNOS) through the c-AMP/protein kinase A pathway [19]. Activation of eNOS is known to contribute to bone marrow cell mobilization, leading to neovascularization [20]. These results raise the possibility that BPS may have beneficial effects on the ischemic myocardium through enhancement of bone marrow cell mobilization.

Thus, the purposes of this study were: (1) to examine the effect of BPS on mobilization and recruitment of bone marrow cells after acute myocardial infarction, (2) to investigate whether BPS induces neovascularization in the ischemic myocardium, and (3) to investigate whether treatment with BPS improves cardiac function in rats with myocardial infarction.

Methods

Model of myocardial infarction. We used male Sprague–Dawley rats (Japan SLC Inc., Hamamatsu, Japan) weighing 185–215 g. Myocardial infarction was produced by left coronary ligation, as described previously [21]. Briefly, after rats were anesthetized with sodium pentobarbital (30 mg/kg), they were artificially ventilated with a volume-regulated respirator. The heart was exposed via a left thoracotomy incision. Then, the left coronary artery was ligated 2–3 mm from its origin between the pulmonary artery conus and the left atrium with a 6-0 Prolene suture. Finally, the heart was restored to its normal position, and the chest was closed. Experimental protocols were performed in accordance with the "Guidelines of the Animal Care Ethics Committee of the National Cardiovascular Center Research Institute", which complies NIH Guidelines.

Administration of BPS. Immediately after coronary ligation, BPS (200 μg/kg/day, Astellas Pharma Inc., Tokyo, Japan) was subcutaneously administered to surviving rats using an osmotic mini-pump for 4 weeks (BPS group, $n = 12$). As a control, saline was similarly administered to rats receiving coronary ligation (Control group, $n = 12$).

Echocardiographic studies. Echocardiographic studies were performed 4 weeks after coronary ligation. M-mode tracings were obtained at the level of the papillary muscles using an echocardiographic system equipped with a 7.5-MHz phased-array transducer (HP SONOS 5500; Hewlett Packard Co., Andover, MA). Anterior and posterior end-diastolic and end-systolic wall thickness, LV end-diastolic and end-systolic dimensions, and LV fractional shortening were measured by the American Society for Echocardiography leading-edge method in three consecutive cardiac cycles. LV meridional wall stress was estimated as $0.344 \times \text{LV pressure} \times \{\text{LV dimension}/(1 + \text{PWT}/\text{LV dimension})\}$, where PWT is posterior wall thickness [22].

Hemodynamic studies. Hemodynamic studies were performed 4 weeks after coronary ligation, following echocardiography. After anesthesia with pentobarbital sodium, a 1.5F micromanometer-tipped catheter (Millar Instruments Inc., Houston, TX) was advanced into the LV through the right common carotid artery. Hemodynamic variables were measured with a pressure transducer connected to a polygraph. After completion of these measurements, the left and right ventricles and the lungs were excised and weighed. Infarct size was determined as a percentage of the entire LV area ($n = 5$ in each group), as reported previously [23]. Briefly, incisions were made in the posterior LV so that the tissue could be pressed flat. The circumference of the entire flat LV and of the visualized infarcted area, as judged from both the epicardial and endocardial sides, was outlined on a clear plastic sheet. The difference in weight between the two marked areas on the sheet was used to determine infarct size and was expressed as a percentage of LV surface area.

Measurement of plasma ANP level. Blood samples were obtained 4 weeks after coronary ligation. Plasma atrial natriuretic peptide (ANP), a marker for heart failure, was measured by enzyme immunoassay (Peninsula Laboratories Inc., San Carlos, CA).

Mononuclear cell mobilization and FACS analysis. To investigate whether administration of BPS mobilizes bone marrow cells, an additional 12 rats were randomized to receive BPS (200 μg/kg/day, BPS group, $n = 6$) or saline (Control group, $n = 6$). On the third day of BPS or saline treatment, 4 ml of blood was drawn from the inferior vena cava of each rat. Peripheral blood was obtained at the end of infusion. After mononuclear cells were counted, they were incubated for 30 min at 4 °C with fluorescein isothiocyanate (FITC)-conjugated mouse monoclonal antibodies against rat CD34 (clone ICO-115, Santa Cruz) and CD45 (clone OX-1), and FITC-conjugated rabbit anti-rat c-Kit polyclonal antibody (clone C-19, Santa Cruz). Immunofluorescence-labeled cells were analyzed by quantitative flow cytometry with a FACSCalibur flow cytometer (BD Biosciences, Mountain View, CA). Isotype-identical antibodies served as controls.

RT-PCR assay. To investigate whether bone marrow cells express the prostacyclin receptor (IP receptor), we analyzed expression of its mRNA by reverse transcription-polymerase chain reaction (RT-PCR). In brief, total RNA of bone marrow cells was extracted with guanidine isothiocyanate (RNeasy Mini Kit, Qiagen). Then, reverse-transcribed single-stranded cDNA was subjected to PCR (PCR Amplification Kit, Takara) using primer sets for the IP receptor (Hokkaido System Science Co., Ltd., Sapporo, Japan, forward, 5′-GGCACGAGAGGATGAAGTTTACC-3′; reverse, 5′-GTCAGAGGCACAGCAGTCAATGG-3′) and G3PDH (Clonetech Laboratories Inc., Mountain View, CA, forward, 5′-TGAAGGTCGGTGTCAACGGATTTGGC-3′; reverse, 5′-CATGTAGGCCATGAGGTCCACCAC-3′).

Creation of bone marrow-chimeric rats. To assess recruitment of bone marrow cells after BPS administration, bone marrow transplantation was performed by using male normal Sprague–Dawley rats as recipients and male Green fluorescent protein (GFP)-transgenic rats (SD-Tg [Act-EGFP] CZ-004Osb, Japan SLC Inc.) as donors, using a previously described method [24]. Briefly, bone marrow was harvested by flushing the cavity of femurs and tibias from GFP-transgenic rats with phosphate-buffered saline. Then, 3×10^7 GFP-positive bone marrow cells were individually administered to 12 lethally irradiated (900 Gray) rats via the tail vein. Four weeks after transplantation, flowcytometric analysis determined that 90% of peripheral blood mononuclear cells from both donors and 8 of 12 chimeric rats were GFP-positive, suggesting the establishment of stable chimerism. These chimeric rats were subjected to left coronary ligation, followed by administration of BPS (200 μg/kg/day, BPS group, $n = 4$) or saline (Control group, $n = 4$) using an osmotic mini-pump for 4 weeks.

Histological examination. To detect fibrosis in the cardiac muscle, the LV myocardium ($n = 5$, each group) was fixed in 10% formalin, cut transversely in three sections, embedded in paraffin, and stained with Masson's trichrome. To detect capillary endothelial cells in the peri-infarct area, we performed DAB staining (LSAB2 System HRP, Dako Cytomation Co., Denmark) using rabbit polyclonal anti-von Willebrand factor (vWF) antibody (Dako). A total of 10 different fields from three different sections were randomly selected, and the number of capillaries was counted in the peri-infarct area using a light microscope at 200× magnification. Capillary density was expressed as the mean number of capillaries per square millimeter. Also, 4 weeks after coronary ligation in bone marrow-chimeric rats ($n = 4$ in each group), the LV myocardium was excised, embedded in OCT compound, snap-frozen in liquid nitrogen, and cut transversely into 6-μm-thick sections from base to apex. Immunofluorescent staining was performed using rabbit polyclonal anti-vWF antibody (Dako), mouse monoclonal anti-cardiac troponin T antibody (Neomarkers, Fremont, CA), and rabbit polyclonal Alexa 488-conjugated anti-GFP antibody (Molecular Probes Inc., Eugene, OR). The nuclei were counterstained with 4′,6′-diamidino-2-phenylindole (DAPI). We measured the number of GFP/vWF-double-positive cells incorporated into vascular structures in 10 randomly selected fields in the peri-infarct area per section in a blinded fashion using a fluorescence microscope.

Statistical analysis. Numerical values are expressed as means ± SEM. Comparisons of parameters between two groups were made by unpaired Student's t test. A value of $p < 0.05$ was considered significant.

Results

Cardiac structure

Body weight at 4 weeks after coronary ligation was significantly greater in the BPS group than in the Control group (Table 1). Right ventricular weight and lung weight in the BPS group were significantly smaller than those in the Control group, although LV weight did not differ between the two groups. Moderate to large infarcts were observed in the Control group (Fig. 1A). However, administration of BPS significantly decreased infarct size in rats with myocardial infarction (Fig. 1A and B). BPS significantly decreased LV end-diastolic dimension (LVDD) (Fig. 1C).

Table 1
Physiological profiles of experimental groups

	Control	BPS
Number	12	12
Body weight (g)		
Baseline	198 ± 3	204 ± 3
After treatment	319 ± 6	352 ± 9*
LV wt/body wt (g/kg)	2.28 ± 0.04	2.27 ± 0.04
RV wt/body wt (g/kg)	0.99 ± 0.05	0.61 ± 0.02**
Lung wt/body wt (g/kg)	6.55 ± 0.62	3.88 ± 0.1**
Plasma AND level (pg/ml)	798 ± 99	498 ± 57*

Control, infarct rats without treatment; BPS, infarct rats treated with BPS administration; AND, atrial natriuretic protein. Data are expressed as means ± SEM. $^{*}p < 0.05$, $^{**}p < 0.01$ vs. Control group.

Cardiac function

Neither heart rate nor mean arterial pressure differed between the BPS and Control groups (Table 2). LV fractional shortening and LV maximum dP/dt in the BPS group were significantly greater than those in the Control group (Fig. 2A and B). LV end-diastolic pressure (LVEDP) in the BPS group was significantly lower than that in the Control group (Fig. 2C). LV minimum dP/dt was also improved by BPS (Fig. 2D). Treatment with BPS attenuated the increase in plasma ANP level after myocardial infarction (Table 1). BPS significantly increased anterior wall thickening, although it did not significantly alter posterior wall thickening (Table 2). Thickness of the anterior and posterior walls tended to be greater in the BPS group, but these changes did not reach statistical significance. LV diastolic wall stress in the BPS group was significantly lower than that in the Control group.

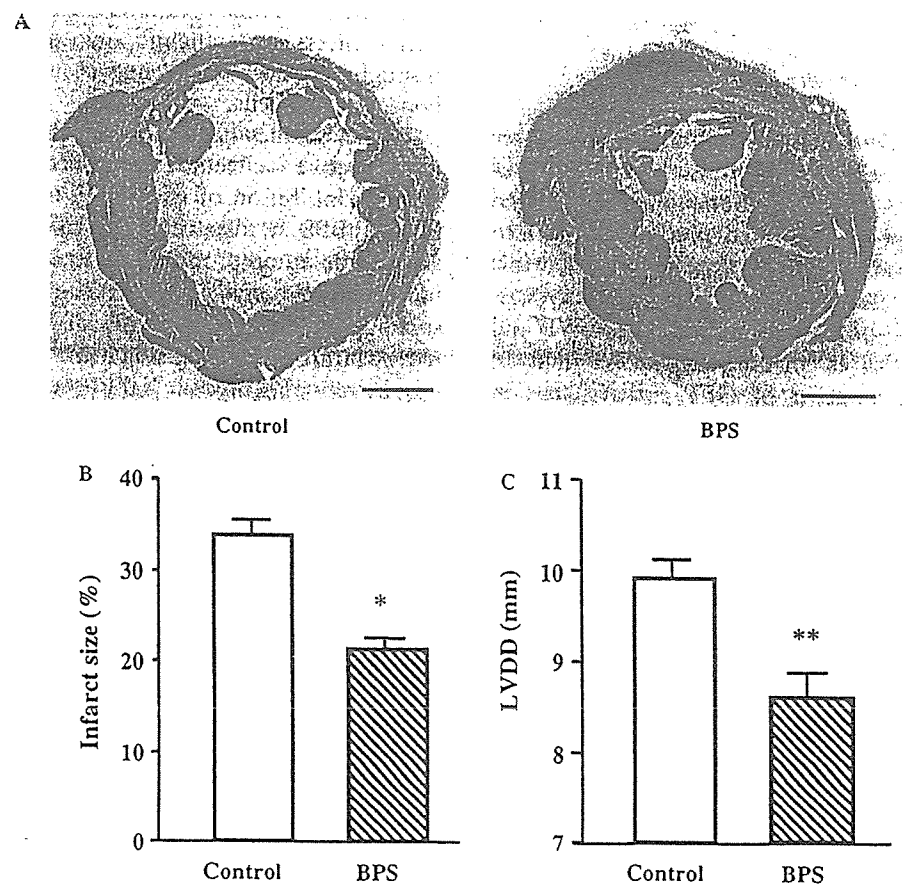

Fig. 1. (A) Representative examples of Masson's trichrome staining of transverse sections of LV myocardium 4 weeks after coronary ligation. Scale bars = 2 mm. (B,C) Quantitative analysis of infarct size and LV end-diastolic dimension (LVDD). Infarcted area and LVDD in the BPS group were significantly smaller than those in the Control group. Data are expressed as means ± SEM. $^{*}p < 0.05$, $^{**}p < 0.01$ vs. Control group.

Table 2
Echocardiographic and hemodynamic data

	Control	BPS
AWT diastole (mm)	0.62 ± 0.04	0.74 ± 0.05
AW thickening (%)	17 ± 3	34 ± 6*
PWT diastole (mm)	1.55 ± 0.07	1.70 ± 0.04
PW thickening (%)	43 ± 4	49 ± 3
Heart rate (bpm)	458 ± 7	471 ± 10
Mean arterial pressure (mmHg)	103 ± 5	115 ± 4
LV systolic pressure (mmHg)	113 ± 4	127 ± 5*
LV diastolic wall stress (kdyne/cm^2)	24 ± 4	5 ± 1**
LV systolic wall stress (kdyne/cm^2)	267 ± 18	225 ± 14

AWT, anterior wall thickness; AW, anterior wall; PWT, posterior wall thickness; PW, posterior wall. Data are expressed as means ± SEM. *$p < 0.05$, **$p < 0.01$ vs. Control group.

Mobilization of bone marrow cells

RT-PCR demonstrated that IP receptor mRNA was expressed in bone marrow cells (Fig. 3A), indicating a direct effect of BPS on these cells. Three-day administration of BPS significantly increased the number of peripheral blood mononuclear cells compared to saline administration (Fig. 3B). Administration of BPS markedly increased the number of circulating progenitor cells such as CD34-positive cells and c-kit-positive cells (Fig. 3C and D). BPS also increased the number of CD45-positive hematopoietic lineage cells (Fig. 3E).

BPS-induced neovascularization

Chimeric rats with GFP-expressing bone marrow were used to assess recruitment of bone marrow cells. Four weeks after coronary ligation, bone marrow-derived GFP-positive cells were incorporated predominantly into the infarcted region and its border zone (Fig. 4A), while these cells were rarely detected in the noninfarcted myocardium. Some of the GFP-positive cells stained for vWF and formed vascular structures. Semi-quantitative analysis demonstrated that the number of GFP-positive cells in the myocardium was significantly greater in the BPS group than in the Control group (Fig. 4B). The number of GFP vWF double-positive cells (bone marrow-derived endothelial cells) in the ischemic myocardium was significantly greater in the BPS group than in the Control group (Fig. 4C). In addition, a small number of GFP-troponin T-double-positive cells were observed in the BPS group (Fig. 4D).

Capillary density

In the peri-infarct area, clustering of relatively small vessels was seen in BPS-treated hearts, which is indicative of recent endothelial regeneration (Fig. 5A). Semi-quantitative analysis also demonstrated that administration of BPS significantly increased the capillary density in the peri-infarct area compared to the Control group (Fig. 5B)

Discussion

In the present study, we demonstrated that treatment with BPS (1) decreased infarct size and improved cardiac structure and function in rats with acute myocardial infarction, (2) increased the number of circulating progenitor cells such as CD34-positive cells and c-kit-positive cells in rats, and (3) increased the number of bone marrow-derived endothelial cells and the capillary density in the ischemic myocardium. These results suggest that BPS may have beneficial effects on ischemic myocardium at least in part through enhancement of neovascularization by mobilizing bone marrow cells.

Earlier studies have reported that prostacyclin has cardioprotective effects in ischemia–reperfusion injury through inhibition of neutrophil activation and migration [25,26]. BPS is also reported to inhibit chemotaxis and superoxide anion production of neutrophils which contribute to tissue damage by releasing tissue destructive lysosomal enzymes [27]. Infusion of BPS has been shown to reduce infarct size in the dog heart with left coronary occlusion by reducing myocardial oxygen demand and by inhibition of the migration of neutrophils [28]. However, these

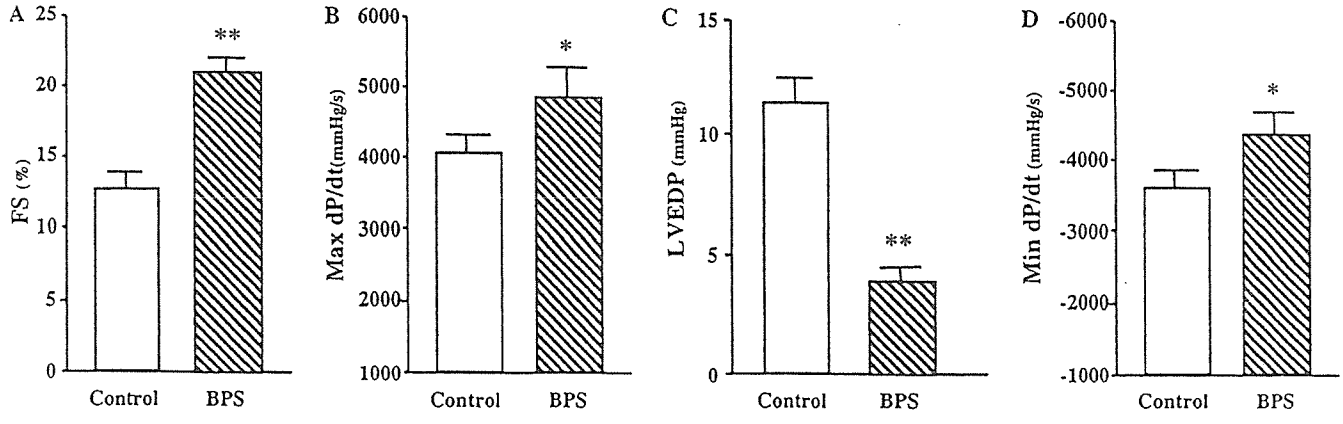

Fig. 2. Cardioprotective effects of BPS on echocardiographic and hemodynamic parameters. FS, fractional shortening; LVEDP, LV end-diastolic pressure; Max and Min dP/dt, maximum and minimum dP/dt. Data are expressed as means ± SEM. *$p < 0.05$, **$p < 0.01$ vs. Control group.

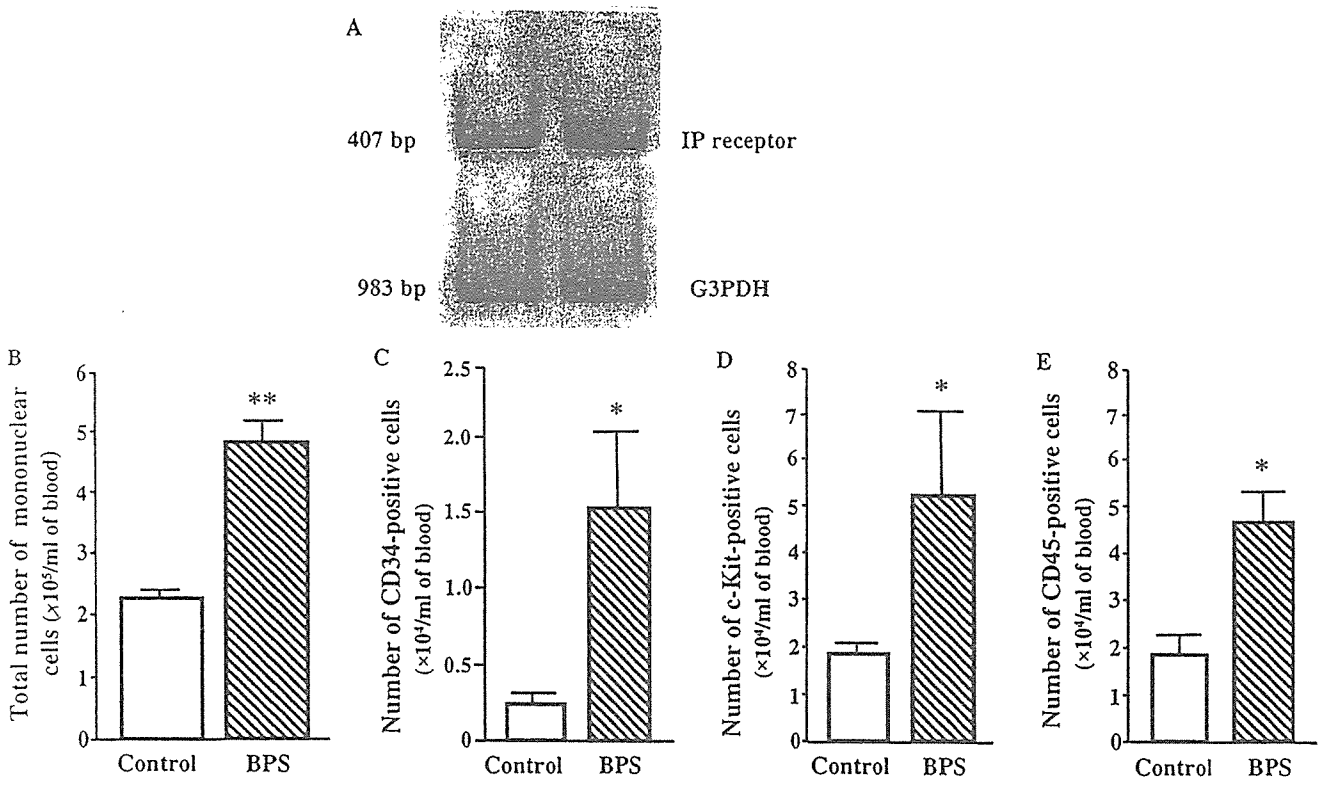

Fig. 3. BPS-induced mobilization of bone marrow cells. (A) Expression of prostacyclin receptor (IP receptor) on bone marrow cells. (B–E) Quantification of BPS-induced MNC mobilization by FACS analysis. Administration of BPS markedly increased the number of circulating progenitor cells such as CD34-positive cells and c-kit-positive cells. BPS also increased the number of CD45-positive hematopoietic lineage cells. Data are expressed as means ± SEM. $^{*}p < 0.05$, $^{**}p < 0.01$ vs. Control group.

biological activities of BPS appear to be insufficient to explain the decrease in infarct size as well as suppression of LV remodeling.

Recent studies have shown that mobilization of bone marrow cells by cytokines promotes myocardial repair and regeneration after acute myocardial infarction [5,6]. In the present study, three-day administration of BPS markedly increased the number of circulating progenitor cells such as CD34-positive cells and c-kit-positive cells in rats. In addition, treatment with BPS enhanced recruitment of bone marrow cells to the ischemic myocardium and increased capillary density in the peri-infarct area. Earlier studies have shown that CD34-positive cells have angiogenic potential to treat ischemic heart [29–31]. Also, another stem cell fraction, c-kit-positive cells have ability to repair ischemic myocardium by differentiating into vascular endothelial cells [32,33]. These findings suggest that administered BPS induces neovascularization partly via enhancement of bone marrow cell mobilization. RT-PCR demonstrated that IP receptor mRNA was expressed in bone marrow cells, indicating a direct effect of BPS on these cells. A recent study has shown that BPS increases eNOS expression in cultured endothelial cells through activation of c-AMP/Protein kinase A signal transduction [19]. Also, earlier studies have shown that eNOS plays essential role in the recruitment of EPCs to the ischemic myocardium [20]. Taken together, administered BPS may act as a potent stimulator of cell mobilization from bone marrow, although further studies are necessary to examine the underlying mechanisms.

In the present study, treatment with BPS significantly attenuated infarct size after myocardial infarction. BPS improved cardiac function and attenuated the development of LV remodeling after acute myocardial infarction, as indicated by increases in LV fractional shortening and maximum dP/dt, and decreases in LVEDP and LVDD. Taken together, BPS may attenuate myocardial infarction through enhancement of neovascularization via modification of bone marrow kinetics. Interestingly, a small fraction of mobilized bone marrow cells expressed cardiac troponin T in the ischemic myocardium in the BPS group, suggesting that BPS may partially contribute to myocardial regeneration after acute myocardial infarction. Earlier studies have demonstrated that BPS has other beneficial effects for ischemic heart disease including anti-thrombotic activity [34], inhibition of reperfusion injury [35], and prevention of coronary spasm [36], and re-stenosis [37]. These findings suggest that administration of BPS may be a promising therapy for acute myocardial infarction.

Granulocyte colony stimulating factor (G-CSF) is currently used agent for mobilization of bone marrow. Infusion of G-CSF after myocardial infarction improves LV function increasing peripheral stem cell fraction [5,38]. A recent clinical trial, however, claimed the G-CSF therapy

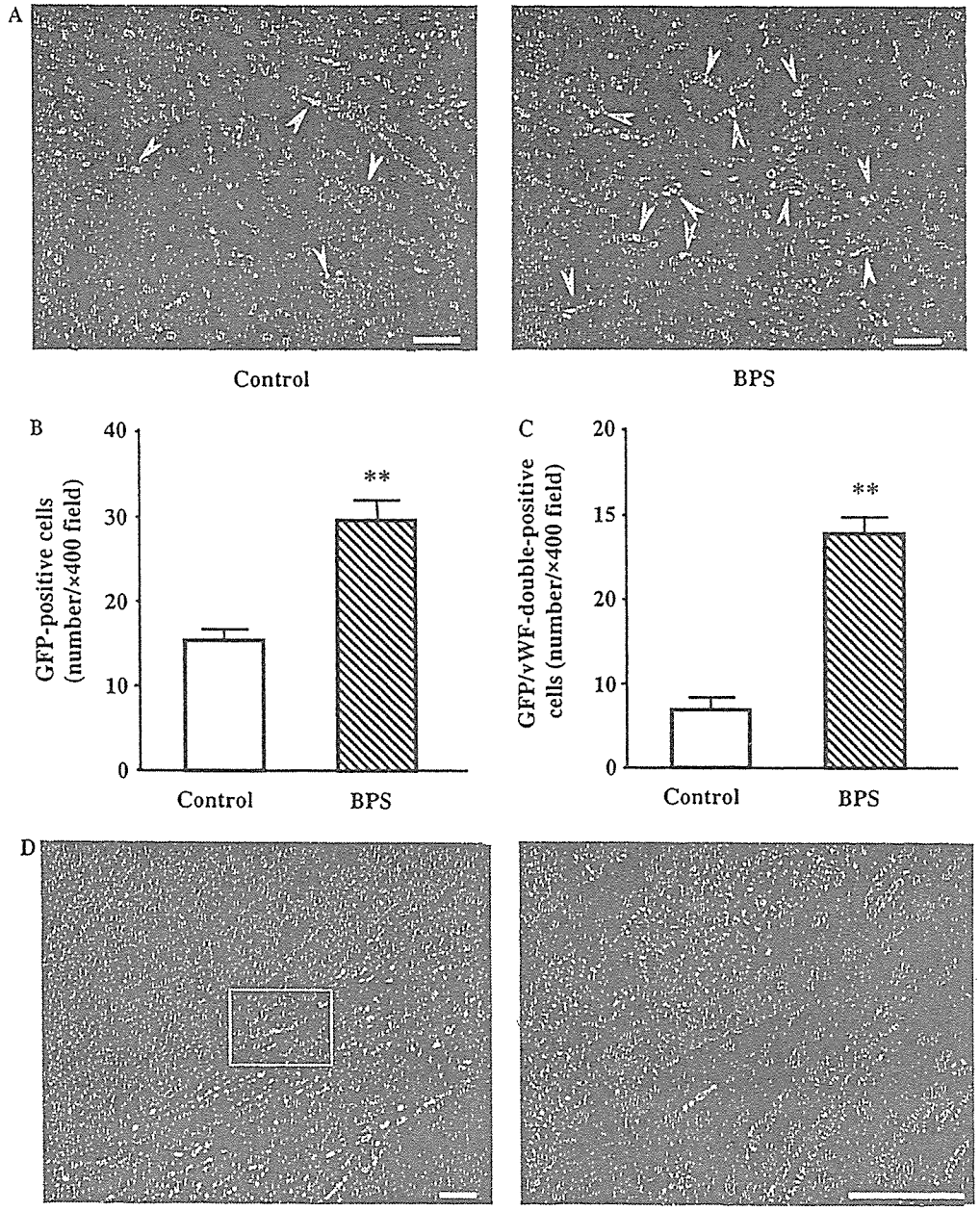

Fig. 4. BPS-induced neovascularization. (A) Representative immunofluorescent images stained with antibodies to von-Willbrand factor (vWF, red) and green fluorescent protein (GFP, green). Nuclei were counterstained with DAPI (blue). (B,C) Semi-quantitative analyses of numbers of GFP-positive cells and GFP-vWF double-positive cells in the peri-infarct area. (D) Representative immunofluorescent image of GFP-positive cells (green) expressing cardiac troponin T (red) observed in the BPS group. Scale bars = 50 μm. Data are expressed as means ± SEM. $^{**}p < 0.01$ vs. Control group.

has serious problem with re-stenosis after recanalization [39]. On the other hand, the safety of BPS has been identified in the treatment of peripheral arterial disease [12,13] and pulmonary arterial hypertension [14,15]. A randomized, controlled clinical trial failed to demonstrate therapeutic potential of prostacyclin for the treatment of severe congestive heart failure [40], which has long discouraged the pursuit of prostacyclin as a therapeutic option for the treatment of acute myocardial infarction. Interestingly, however, double-blinded, randomized, placebo-controlled, large-scale studies showed that treatment with BPS decreased vascular events in patients with peripheral arterial disease [41,42]. Thus, adequate use of BPS for only acute myocardial infarction may have beneficial effects on ischemic myocardium, although further preclinical trials are required to verify the safety and efficacy of BPS.

Conclusion

In summary, administration of BPS improved cardiac structure and function in rats with acute myocardial infarction. This beneficial effect of BPS may be mediated partly by its ability to enhance neovascularization in ischemic myocardium by mobilizing bone marrow cells.

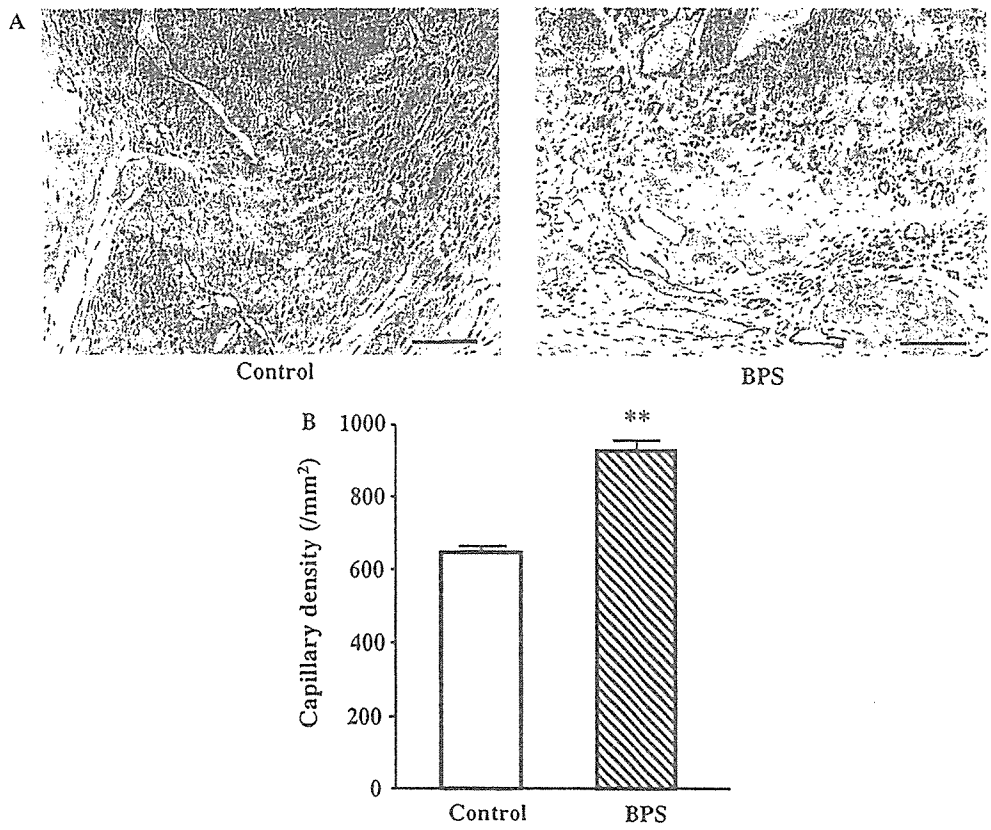

Fig. 5. (A) Representative samples stained with antibody to von Willebrand factor by bright-field DAB. (B) Quantitative analysis of capillary density in peri-infarct area. Administration of BPS increased capillary density by 37%. Scale bars = 50 μm. Data are expressed as means ± SEM. $^{**}p < 0.01$ vs. Control group.

Acknowledgment

This work was supported by research grants for Cardiovascular Disease (16C-6) from the Ministry of Health, Labor and Welfare, and for Japan Vascular Disease Research Foundation.

References

[1] A. Saraste, K. Pulkki, M. Kallajoki, K. Henriksen, M. Parvinen, L.M. Voipio-Pulkki, Apoptosis in human acute myocardial infarction, Circulation 95 (1997) 320–323.
[2] S. Shintani, T. Murohara, H. Ikeda, T. Ueno, T. Honma, A. Katoh, K. Sasaki, T. Shimada, Y. Oike, T. Imaizumi, Mobilization of endothelial progenitor cells in patients with acute myocardial infarction, Circulation 103 (2001) 2776–2779.
[3] D. Orlic, J. Kajstura, S. Chimenti, I. Jakoniuk, S.M. Anderson, B. Li, J. Pickel, R. Mckay, B. Nadal-Ginard, D.M. Bodine, A. Leri, P. Anversa, Bone marrow cells regenerate infarcted myocardium, Nature 410 (2001) 701–705.
[4] H. Oh, S.B. Bradfute, T.D. Gallardo, T. Nakamura, V. Gaussin, Y. Mishina, J. Pocius, L.H. Michael, R.R. Behringer, D.J. Garry, M.L. Entman, M.D. Schneider, Cardiac progenitor cells from adult myocardium: homing, differentiation, and fusion after infarction, Proc. Natl. Acad. Sci. USA 100 (2003) 12313–12318.
[5] D. Orlic, J. Kajstura, S. Chimenti, F. Limana, I. Jakoniuk, F. Quaini, B. Nadal-Ginard, D.M. Bodine, A. Leri, P. Anversa, Mobilized bone marrow cells repair the infarcted heart, improving function and survival, Proc. Natl. Acad. Sci. USA 98 (2001) 10344–10349.
[6] T. Asahara, T. Takahashi, H. Masuda, C. Kalka, D. Chen, H. Iwaguro, Y. Inai, M. Silver, J.M. Isner, VEGF contributes to postnatal neovascularization by mobilizing bone marrow-derived endothelial progenitor cells, EMBO J. 18 (1999) 3964–3972.
[7] T. Murata, T. Murai, T. Kanai, Y. Ogaki, K. Sanai, H. Kanda, S. Sato, N. Kajikawa, T. Umetsu, H. Matsuura, General pharmacology of beraprost sodium, Arzneimittelforschung 39 (1989) 867–876.
[8] T. Akiba, M. Miyazaki, N. Toda, Vasodilator actions of TRK-100, a new prostaglandin I2 analogue, Br. J. Pharmacol. 89 (1986) 703–711.
[9] S. Nishio, H. Matsuura, N. Kanai, Y. Fukatsu, T. Hirano, N. Nishikawa, K. Kameoka, T. Umetsu, The in vitro and ex vivo antiplatelet effect of TRK-100, a stable prostacyclin analog, in several species, Jpn J. Pharmacol. 47 (1988) 1–10.
[10] J.L. Demolis, A. Robert, M. Mouren, C. Funck-Brentano, P. Jaillon, Pharmacokinetics and platelet antiaggregating effects of beraprost, an oral stable prostacyclin analogue, in healthy volunteers, J. Cardiovasc. Pharmacol. 22 (1993) 711–716.
[11] P. Nony, P. Ffrench, P. Girard, S. Delair, S. Azoulay, J.P. Girre, M. Dechavanne, J.P. Boissel, Platelet-aggregation inhibition and hemodynamic effects of beraprost sodium, a new oral prostacyclin derivative: a study in healthy male subjects, Can. J. Physiol. Pharmacol. 74 (1996) 887–893.
[12] M. Murakami, M. Watanabe, H. Furukawa, H. Nakahara, The prostacyclin analogue beraprost sodium prevents occlusion of bypass grafts in patients with lower extremity arterial occlusive disease: a 20-year retrospective study, Ann. Vasc. Surg. 19 (2005) 838–842.
[13] L.T. Cooper, Beraprost for the treatment of intermittent claudication, J. Am. Coll. Cardiol. 41 (2003) 1679–1686.
[14] Y. Okano, T. Yoshioka, A. Shimouchi, T. Satoh, T. Kunieda, Orally active prostacyclin analogue in primary pulmonary hypertension, Lancet 349 (1997) 1365.

[15] N. Nagaya, M. Uematsu, Y. Okano, T. Satoh, S. Kyotani, F. Sakamaki, N. Nakanishi, K. Miyatake, T. Kunieda, Effect of orally active prostacyclin analogue on survival of outpatients with primary pulmonary hypertension, J. Am. Coll. Cardiol. 34 (1999) 1188–1192.
[16] A.M. Lefer, M.L. Ogletree, J.B. Smith, M.J. Silver, K.C. Nicolaou, [illegible] G P. Gasic, Prostacyclin: a potentially valuable agent [illegible] myocardial ischemia, Science 200 (1978) 52–54.
[17] B.L. Jugdutt, G.M. Hutchins, B.H. Bulkley, L.C. Becker, Dissimilar effects of prostacyclin, prostaglandin E1, and prostaglandin E2 on myocardial infarct size after coronary occlusion in conscious dogs, Circ. Res. 49 (1981) 685–700.
[18] J.A. Melin, L.C. Becker, Salvage of ischemic myocardium by prostacyclin during experimental myocardial infarction, J. Am. Coll. Cardiol. 2 (1983) 279–286.
[19] K. Niwano, M. Arai, K. Tomaru, T. Uchiyama, Y. Ohyama, M. Kurabayashi, Transcriptional stimulation of the eNOS gene by the stable prostacyclin analogue beraprost is mediated through cAMP-responsive element in vascular endothelial cells: close link between PGI2 signal and NO pathways, Circ. Res. 93 (2003) 523–530.
[20] A. Aicher, C. Heeschen, C. Mildner-Rihm, C. Urbich, C. Ihling, K. Technau-Ihling, A.M. Zeiher, S. Dimmeler, Essential role of endothelial nitric oxide synthase for mobilization of stem and progenitor cells, Nat. Med. 9 (2003) 1370–1376.
[21] T. Nishikimi, K. Uchino, E.D. Frohlich, Effects of α1-adrenergic blockade on intrarenal hemodynamics in heart failure rats, Am. J. Physiol. Regul. Integr. Comp. Physiol. 262 (1998) R198–R203.
[22] P.S. Douglas, N. Reichek, T. Plappert, A. Muhammad, M.G. St John Sutton, Comparison of echocardiographic methods for assessment of left ventricular shortening and wall stress, J. Am. Coll. Cardiol. 9 (1987) 945–951.
[23] Y.W. Chien, R.W. Barbee, A.A. Macphee, E.D. Frohlich, N.C. Trippondo, Increased ANF secretion after volume expansion is preserved in rats with heart failure, Am. J. Physiol. 254 (1988) R185–R191.
[24] T. Ito, A. Suzuki, E. Imai, M. Okabe, M. Hori, Bone marrow is a reservoir of repopulating mesangial cells during glomerular remodeling, J. Am. Soc. Nephrol. 12 (2001) 2625–2635.
[25] P.J. Simpson, R.F. Todd 3rd, J.C. Fantone, J.K. Mickelson, J.D. Griffin, B.R. Lucchesi, Reduction of experimental canine myocardial reperfusion injury by a monoclonal antibody (anti-Mo1, anti-CD11b) that inhibits leukocyte adhesion, J. Clin. Invest. 81 (1988) 624–629.
[26] W.W. Nichols, J. Mehta, T.J. Wargovich, D. Franzini, D. Lawson, Reduced myocardial neutrophil accumulation and infarct size following thromboxane synthetase inhibitor or receptor antagonist, Angiology 40 (1989) 209–221.
[27] M. Kainoh, R. Imai, T. Nakadake, M. Hattori, S. Nishio, Prostacyclin and beraprost sodium as suppressors of activated rat polymorphonuclear leukocytes, Biochem. Pharmacol. 39 (1990) 477–483.
[28] Y. Ueno, Y. Miyauchi, S. Nishio, Beraprost sodium protects occlusion/reperfusion injury in the dog by inhibition of neutrophil migration, Gen. Pharmacol. 25 (1994) 427–432.
[29] A. Kawamoto, T. Tkebuchava, J. Yamaguchi, H. Nishimura, Y.S. Yoon, C. Milliken, S. Uchida, O. Masuo, H. Iwaguro, H. Ma, A. Hanley, M. Silver, M. learney, D.W. Losordo, J.M. Isner, T. Asahara, Intramyocardial transplantation of autologous endothelial progenitor cells for therapeutic neovascularization of myocardial ischemia, Circulation 107 (2003) 461–468.
[30] A. Kawamoto, T. Asahara, D.W. Losordo, Transplantation of endothelial progenitor cells for therapeutic neovascularization, Cardiovasc. Radiat. Med. 3 (2002) 221–225.
[31] A. Weber, I. Pedrosa, A. Kawamoto, N. Himes, J. Munasinghe, T. Asahara, N.M. Rofsky, D.W. Losordo, Magnetic resonance mapping of transplanted endothelial progenitor cells for therapeutic neovascularization in ischemic heart disease, Eur. J. Cardiothorac. Surg. 26 (2004) 137–143.
[32] J. Kajstura, M. Rota, B. Whang, S. Cascapera, T. Hosoda, C. Bearzi, D. Nurzynska, H. Kasahara, E. Zias, M. Bonafe, B. Nadal-Ginard, D. Torella, A. Nascimbene, F. Quaini, K. Urbanek, A. Leri, P. Anversa, Bone marrow cells differentiate in cardiac cell lineages after infarction independently of cell fusion, Circ. Res. 96 (2005) 127–137.
[33] R. Lanza, M.A. Moore, T. Wakayama, A.C. Perry, J.H. Shieh, J. Hendrikx, A. Leri, S. Chimenti, A. Monsen, D. Nurzynska, M.D. West, J. Kajstura, P. Anversa, Regeneration of the infarcted heart with stem cells derived by nuclear transplantation, Circ. Res. 94 (2004) 820–827.
[34] Y. Uchida, T. Hanai, K. Hasegawa, K. Kawamura, T. Oshima, Recanalization of obstructed coronary artery by intracoronary administration of prostacyclin in patients with acute myocardial infarction, Adv. Prostaglandin Thromboxane Leukot. Res. 11 (1983) 377–383.
[35] C.Y. Xiao, A. Hara, Yuhki K, T. Fujino, H. Ma, Y. Okada, O. Takahata, T. Yamada, T. Murata, S. Narumiya, F. Ushikubi, Roles of prostaglandin I(2) and thromboxane A(2) in cardiac ischemia–reperfusion injury: a study using mice lacking their respective receptors, Circulation 104 (2001) 2210–2215.
[36] A. Szczeklik, J. Szczeklik, R. Nizankowski, P. Gluszko, Prostacyclin for unstable angina, N. Engl. J. Med. 303 (1980) 881.
[37] M.L. Knudtson, V.F. Flintoft, D.L. Roth, J.L. Hansen, H.J. Duff, Effect of short-term prostacyclin administration on restenosis after percutaneous transluminal coronary angioplasty, J. Am. Coll. Cardiol. 15 (1990) 691–697.
[38] F. Kuethe, H.R. Figulla, M. Herzau, M. Voth, M. Fritzenwanger, T. Opfermann, K. Pachmann, A. Krack, H.G. Sayer, D. Gottschild, G.S. Werner, Treatment with granulocyte colony-stimulating factor for mobilization of bone marrow cells in patients with acute myocardial infarction, Am. Heart J. 150 (2005) 115.
[39] H.J. Kang, H.S. Kim, S.Y. Zhang, K.W. Park, H.J. Cho, B.K. Koo, Y.J. Kim, D. Soo Lee, D.W. Sohn, K.S. Han, B.H. Oh, M.M. Lee, Y.B. Park, Effects of intracoronary infusion of peripheral blood stem-cells mobilised with granulocyte-colony stimulating factor on left ventricular systolic function and restenosis after coronary stenting in myocardial infarction: the MAGIC cell randomised clinical trial, Lancet 363 (2004) 751–756.
[40] R.M. Califf, K.F. Adams, W.J. McKenna, M. Gheorghiade, B.F. Uretsky, S.E. McNulty, H. Darius, K. Schulman, F. Zannad, E. Handberg-Thurmond, F.E. Harrell Jr., W. Wheeler, J. Soler-Soler, K. Swedberg, A randomized controlled trial of epoprostenol therapy for severe congestive heart failure: The Flolan International Randomized Survival Trial (FIRST), Am. Heart J. 134 (1997) 44–54.
[41] M. Lievre, S. Morand, B. Besse, J.N. Fiessinger, J.P. Boissel, Oral beraprost sodium, a prostaglandin I(2) analogue, for intermittent claudication: a double-blind, randomized, multicenter controlled trial. Beraprost et Claudication Intermittente (BERCI) Research Group, Circulation 102 (2000) 426–431.
[42] E.R. Mohler 3rd, W.R. Hiatt, J.W. Olin, M. Wade, R. Jeffs, A.T. Hirsch, Treatment of intermittent claudication with beraprost sodium, an orally active prostaglandin I2 analogue: a double-blinded, randomized, controlled trial, J. Am. Coll. Cardiol. 41 (2003) 1679–1686.

nature medicine

Monolayered mesenchymal stem cells repair scarred myocardium after myocardial infarction

Yoshinori Miyahara[1,9], Noritoshi Nagaya[1,9], Masaharu Kataoka[1], Bobby Yanagawa[1], Koichi Tanaka[1], Hiroyuki Hao[2], Kozo Ishino[3], Hideyuki Ishida[4], Tatsuya Shimizu[5], Kenji Kangawa[6], Shunji Sano[3], Teruo Okano[5], Soichiro Kitamura[7] & Hidezo Mori[8]

Mesenchymal stem cells are multipotent cells that can differentiate into cardiomyocytes and vascular endothelial cells. Here we show, using cell sheet technology, that monolayered mesenchymal stem cells have multipotent and self-propagating properties after transplantation into infarcted rat hearts. We cultured adipose tissue–derived mesenchymal stem cells characterized by flow cytometry using temperature-responsive culture dishes. Four weeks after coronary ligation, we transplanted the monolayered mesenchymal stem cells onto the scarred myocardium. After transplantation, the engrafted sheet gradually grew to form a thick stratum that included newly formed vessels, undifferentiated cells and few cardiomyocytes. The mesenchymal stem cell sheet also acted through paracrine pathways to trigger angiogenesis. Unlike a fibroblast cell sheet, the monolayered mesenchymal stem cells reversed wall thinning in the scar area and improved cardiac function in rats with myocardial infarction. Thus, transplantation of monolayered mesenchymal stem cells may be a new therapeutic strategy for cardiac tissue regeneration.

Myocardial infarction, a main cause of heart failure, leads to loss of cardiac tissue and impairment of left ventricular function. Therefore, restoring the scarred myocardium is desirable for the treatment of heart failure. Although needle injections of bone marrow cells into the myocardium have been performed for cardiac regeneration[1–5], it is difficult to reconstruct sufficient cardiac mass in the thinned scar area after myocardial infarction.

Recently, our colleagues have developed cell sheets using temperature-responsive culture dishes[6]. These cell sheets allow for cell-to-cell connections and maintain the presence of adhesion proteins because enzymatic digestion is not needed[7–10]. Therefore, cell sheet transplantation may be a promising strategy for partial cardiac tissue reconstruction. Skeletal myoblasts, fetal cardiomyocytes and embryonic stem cells have been considered as candidates for an implantable cell source[11–13]. It is difficult, however, to produce a multilayered construct requiring a vascular network. Thus, autologous somatic stem cells with self-propagating properties that can induce angiogenesis are a desirable cell source for a transplantable sheet.

Mesenchymal stem cells (MSCs) are multipotent adult stem cells that reside within the bone marrow microenvironment[14,15]. MSCs can differentiate not only into osteoblasts, chondrocytes, neurons and skeletal muscle cells, but also into vascular endothelial cells[16] and cardiomyocytes[17–20]. In contrast to their hematopoietic counterparts, MSCs are adherent and can expand in culture. Recently, MSCs have been isolated from adipose tissue[21–24], which is typically abundant in individuals with cardiovascular disease. Here, we investigated the therapeutic potency of monolayered MSCs derived from adipose tissue using cell sheet technology.

RESULTS

Characteristics of adipose tissue–derived MSCs

We isolated MSCs from subcutaneous adipose tissue of male Sprague-Dawley rats on the basis of the adherent properties of these cells. We obtained $1.7 \times 10^5 \pm 0.2 \times 10^5$ cells from 1 g adipose tissue in a 12-h culture. By day 4 of culture of the minced adipose tissue, spindle-shaped adherent cells were apparent and formed symmetric colonies. After approximately three to four passages, most adherent cells expressed CD29 and CD90 (**Supplementary Fig. 1** online). In contrast, the majority of adherent cells were negative for CD34 and CD45. They were also negative for CD31, a marker for vascular endothelial cells, and negative for α smooth muscle actin (αSMA), a marker for smooth muscle cells. A small fraction of adherent cells expressed CD71, CD106 and CD117. These results were similar to those from bone marrow–derived MSCs[15,22,25] (**Supplementary Fig. 1** online). Using previously described methods[16,22,26], we confirmed that these adipose-derived adherent cells, like bone marrow–derived MSCs, were multipotent, as judged by their ability to differentiate into adipocytes, osteoblasts and vascular endothelial cells. Thus, we

[1]Department of Regenerative Medicine and Tissue Engineering, National Cardiovascular Center Research Institute and [2]Department of Pathology, National Cardiovascular Center, 5-7-1 Fujishirodai, Suita, Osaka, 565-8565, Japan. [3]Department of Cardiovascular Surgery, Okayama University Graduate School of Medicine, Dentistry and Pharmaceutical Sciences, 2-5-1 Shikata-cho, Okayama, 700-8555, Japan. [4]Department of Physiology, School of Medicine, Tokai University, Bohseidai, Isehara, Kanagawa, 259-1193, Japan. [5]Institute of Advanced Biomedical Engineering and Science, Tokyo Woman's Medical University, 8-1 Kawada-cho, Shinjuku-ku, Tokyo, 162-8666, Japan. [6]Department of Biochemistry, National Cardiovascular Center Research Institute and [7]Department of Cardiovascular Surgery, National Cardiovascular Center and [8]Department of Cardiac Physiology, National Cardiovascular Center Research Institute, 5-7-1 Fujishirodai, Suita, Osaka, 565-8565, Japan. [9]These authors contributed equally to this work. Correspondence should be addressed to N.N. (nnagaya@ri.ncvc.go.jp) or H.M. (hidemori@ri.ncvc.go.jp).

Received 9 August 2005; accepted 3 March 2006; published online 2 April 2006; doi:10.1038/nm1391